Lockett, R. D., Ball, D. & Robertson, G. (2013). Experimental cross-correlation Nitrogen Q-branch CARS Thermometry in a Spark Ignition Engine. Optics and Lasers in Engineering,

CITY UNIVERSITY LONDON

City Research Online

Experimental Cross-Correlation Nitrogen Q-branch CARS Thermometry in a Spark Ignition Engine

*R.D. Lockett[1], D. Ball, G.N. Robertson

Department of Physics, University of Cape Town, Rondebosch 7700, Republic of South Africa

[1]Now based at: School of Engineering & Mathematical Sciences, City University London, Northampton Square, London, EC1V 0HB, UK

Abstract

A purely experimental technique was employed to derive temperatures from nitrogen Q-branch Coherent Anti-Stokes Raman Scattering (CARS) spectra, obtained in a high pressure, high temperature environment (spark ignition Otto engine). This was in order to obviate any errors arising from deficiencies in the spectral scaling laws which are commonly used to represent nitrogen Q-branch CARS spectra at high pressure. The spectra obtained in the engine were compared with spectra obtained in a calibrated high pressure, high temperature cell, using direct cross-correlation in place of the minimisation of sums of squares of residuals.

The technique is demonstrated through the measurement of air temperature as a function of crankshaft angle inside the cylinder of a motored single-cylinder Ricardo E6 research engine, followed by the measurement of fuel-air mixture temperatures obtained during the compression stroke in a knocking Ricardo E6 engine. A standard CARS program (SANDIA's CARSFIT) was employed to calibrate the altered non-resonant background contribution to the CARS spectra that was caused by the alteration to the mole fraction of nitrogen in the unburned fuel-air mixture. The compression temperature profiles were extrapolated in order to predict the auto-ignition temperatures.

Keywords: CARS; thermometry; auto-ignition; engine, cross-correlation

Highlights:

1. Normalised cross-correlation facilitates quantitative comparison of spectra.
2. A high pressure, high temperature cell has been used to generate a spectra database.
3. An experimental method has been developed to measure engine cylinder temperature.
4. Compression temperature profiles during knock for methanol and coal-to-liquid gasoline.

*Corresponding Author: Email: r.d.lockett@city.ac.uk
Tel. 44 (0)207 040 8812
Fax. 44 (0)207 040 8566

1. Introduction

Conventional nitrogen CARS thermometry normally involves the comparison of sets of referenced single-shot and/or averaged experimental broad-band nitrogen CARS Q-branch spectra obtained from a combustion environment, with a database of computed nitrogen CARS Q-branch profiles [1 – 6]. The quantitative comparison of experimental spectra with modelled spectra is normally achieved through a minimisation of the sum of squared differences. The database of spectral profiles is usually determined for a specified range of temperatures, pressure and gas composition, and consists of sets of spectra computed at discrete intervals over a wide range of temperature [3 – 5].

The use of a model computed database of CARS spectra in order to determine gas temperature distributions and/or profiles (as outlined above) in combustion environments is the most common methodology employed for CARS based gas temperature measurements. It has been employed in the experimental determination of temperature in many different combustion environments, including laboratory burners [7 – 10], internal combustion engines [11 – 17], rocket and gas turbine combustors and exhausts [18 – 21], and furnaces [22 – 24].

Two surveys of many nitrogen Q-branch CARS thermometry experiments reported in 1996 and 2002 respectively, revealed that the typical relative precision achieved was approximately 3 % (percentage standard deviation to mean ratio) for averaged spectra and approximately 10% uncertainty for single-shot measurements [25, 26].

More recently, developments in nano-second (ns) CARS have focussed on the extension of capability to permit multiple-species measurement, together with temperature, and to higher pressures [27]. In addition, measurement accuracy and precision associated with rotational CARS has improved in the 300 K to 1,000 K temperature range, achieving an accuracy to rival or even surpass the accuracy achievable in vibrational CARS.

The precision achievable in nitrogen Q-branch CARS thermometry has improved to offer a minimum single-shot experimental uncertainty in measured temperature of

approximately ± 15 K to ± 25 K (one standard deviation of CARS temperature distribution) in the 300 K to 1,000 K range of temperature, and approximately 2.5 % relative uncertainty for single shot temperature measurements above 1,000 K [27]. The improvement in CARS measurement precision has developed through improvements to rotational CARS, and the development and use of modeless dye lasers (which removes the spectral noise arising from dye laser mode competition) [28, 29]. Of course, this level of precision applies to nearly perfectly heated calibrated environments (calibrated heated cells, and calibrated flames). However, the complexities found in realistic combustion environments (engines, combustors, furnaces) results in reduced measurement precision.

The accuracy associated with the collisional models available for nitrogen, together with the variation in experimentally obtained nitrogen CARS spectra, results in a net minimum error of approximately 20 K in the range of temperatures and pressures of 500 K to 1,000 K, and 0.1 MPa to 2.0 MPa respectively [27]. An example of CARS measurement accuracy as a function of pressure was presented in the paper of Bood *et al.* [30]. They have presented rotational CARS temperature measurements conducted in a calibrated cell at 295 K, for pressures ranging from 0.1 MPa to 44 MPa, using various collisional models (modified exponential gap (MEG), energy corrected sudden approximation (ECS), and semi-classical collision (SCL) models). The results showed a difference of up to 10 K in the range of pressures from 0.1 MPa to 2.0 MPa, and up to 18 K in the range of pressures from 2.0 MPa to 7.5 MPa.

This was followed by the work of Afzelius *et al.* [31], which introduced improvements to S-branch Raman line-widths and included the effect of inter-branch interference to the models for the calculation of database CARS spectra. This led to an improvement in relative measurement error to approximately 2.5 % at 295 K over the 1 MPa to 7 MPa pressure range.

More recently, Kliewer *et al.* [32] have conducted an analysis of the accuracy of rotational CARS models (modified exponential gap (MEG) and energy corrected sudden approximation (ECS) models) in comparison with thermocouple measurements obtained from a calibrated high temperature cell at atmospheric pressure, in the temperature range of 300 K to 1,400 K. They showed that the

rotational CARS models were capable of predicting the cell temperature with a relative error of approximately 2 % in the temperature range of 600 K to 1,000 K.

These examples indicate that the smallest achievable relative error presently associated with the computational models employed for CARS thermometry is approximately 2 % to 3 % in the temperature and pressure range of 295 K to 1,500 K and 0.1 MPa to 7 MPa respectively. This is particularly important in the context of measurements in the cylinders of internal combustion engines, which undergo varying temperature and pressure conditions over the range identified above.

A number of recent examples of CARS temperature measurements in engines have employed rotational CARS. Grandin *et al.* [33] employed rotational CARS in order to determine the temperature in the thermal boundary layer of an engine subjected to knocking and normal operation, in order to contrast the temperature profiles and heat transfer occurring during knocking and normal operation. Weikl *et al.* [34] employed rotational CARS in order to determine temperature and gas composition in a homogeneous charge compression ignition engine. The authors also employed a pulse stretching system in this study, which was developed earlier and reported elsewhere [35]. The use of a pulse-stretching CARS system for these engine measurements eliminated the possibility of optical damage to the windows, and improved the measurement precision, through an increase in signal-to-noise-ratio. They obtained standard deviations of approximately 50 K from the distributions of CARS temperatures obtained from the HCCI engine.

More recently, Birkigt *et al.* [36] have employed rotational CARS for the measurement of temperature in a motored and butane-fuelled firing engine, for the purpose of improving the determination of compression temperature. They were able to achieve standard deviations in the CARS temperature distributions of 17 K during motoring, and 25 K during firing operation respectively. This is to be compared with an achievable standard deviation of approximately 12 K in a calibrated oven.

As stated earlier, the comparison of the averaged spectra and sets of single-shot spectra is usually performed numerically using non-linear least squares techniques. However, there are some theoretical objections and practical limitations to the non-

linear least squares method in CARS spectroscopy. Least squares minimisation is statistically valid only if the measurement variations are normally distributed and are uncorrelated. The practical limitations are encountered when the experimental data has a high noise level. The normal equations are non-linear, and therefore finding the least squares minimum is computationally time-consuming, and must satisfy rigorous convergence criteria. Experimental data with high noise levels will sometimes not satisfy the convergence criteria, and may lead to the discovery of many local minima occurring in the neighbourhood of the true minimum.

This paper presents a simpler and quicker numerical method of comparing sets of spectra. The method uses a normalised cross-correlation technique that is formally equivalent to the normalised non-linear least squares technique. The normalised cross-correlation function possesses useful Fourier transform properties, which facilitate fast computation of cross-correlations of many spectra, and provides an objective measure of goodness-of-fit during the comparison of spectra.

The cross-correlation function was derived for use in mathematical statistics, in order to identify correlations between apparently random variables (cross-covariance of probability density functions). It is also employed in acoustics and plasma physics as a means of comparing transmitted and reflected acoustic pulses with the source pulse for the purpose of determining time of flight, and the medium transfer function. It is capable of retaining useful phase information between two waveforms, and facilitates the determination of the speed of sound and the dispersion relation in a dispersive medium.

The cross-correlation function was employed by Lockett [37] to compare experimental CARS spectra with a spectral database for the determination of gas temperature. It was quickly realized that the cross-correlation function had useful Fourier properties, enabling the fast numerical comparison of many spectra. The use of Fourier techniques to compute the normalised cross-correlation for fast fitting of experimental vibrational CARS spectra was described in a short paper by Robertson and Roblin [38], where they discussed the potential benefits of fast computation of many normalised cross-correlations using dedicated Fast Fourier Transform (FFT)

processors against the conventional Marquardt-Levenberg minimisation of sums of squares of residuals.

Schenk *et al.* [39] have since employed the cross-correlation technique in a comparative study of various fitting techniques to be employed in rotational CARS. They compared a Fourier analysis technique (FAT), cross-correlation, and four variations of weighted least squares techniques in fitting rotational CARS spectral profiles obtained from a calibrated heated cell. They concluded that the constant weighted and the inverse weighted least squares techniques provided the best options in terms of accuracy and precision. They found that the cross-correlation technique offered good applicability to experiments subject to strong optical distortions, as the technique proved robust to spectral shifts. It is interesting to note that the rotational CARS temperature measurements utilising all six of the fitting methods produced CARS temperature distributions with a mean uncertainty of 0.03 (approximately 3 % variation from the cell temperature), and a standard deviation to mean temperature ratio of 0.05 to 0.07 (5 % to 7 %).

This paper also introduces an alternative experimental methodology for conducting broad-band nitrogen CARS thermometry. The methodology consisted of creating a database of referenced broad-band nitrogen Q-branch spectra from inside a calibrated high-pressure high-temperature (HPHT) cell. The database of experimental spectra obtained from the HPHT cell can then be employed for comparison with spectra obtained from an unknown combustion environment, and hence the determination of temperature in the unknown combustion environment. We report the application of this methodology to the measurement of temperature during the compression stroke in a motored and knocking optically accessible Ricardo E6 engine.

This form of empirical CARS thermometry was limited to the temperature and pressure range obtained in the HPHT cell. The experimental uncertainty in the determination of temperature was principally determined by the experimental uncertainty obtained in the HPHT cell. However, this form of CARS thermometry is independent of the uncertainties contained in the modelled form of the nitrogen CARS non-linear susceptibility.

Optical cells have previously been employed for the calibration of CARS based concentration measurements, and of course, have been used widely for temperature calibration of CARS models [5, 26 - 28, 30 - 32, 34]. Green *et al.* [40] employed an optical cell with known concentrations of gases, in order to determine the gas concentrations obtained in the burned gas of a firing engine. Beyrau *et al.* [41] have utilized a heated gas cell as part of a dual-pump CARS experiment applied in a partially premixed ethene-air jet flame in order to determine the local nitrogen-ethene ratio. This formed part of a more comprehensive set of measurements including local nitrogen-oxygen concentration, together with local gas temperature.

The experimental work reported here was conducted twenty years ago, employing CARS equipment and methods that might appear somewhat dated. In-cylinder engine temperature profiles similar to those presented here have been published previously by the authors [42]. However, the experimental methodology and the spectral fitting method that was developed has not previously been published, and produced CARS engine temperature profiles with an accuracy and precision that remain comparable with recent experiments. Birkigt *et al.* [36] state that rotational CARS temperature measurements are capable of achieving temperature measurements with a maximum error of approximately 55 K in the temperature range 300 K to 1,600 K. Kliewer *et al.* [32] have reported that they were able to achieve temperature measurements with a maximum error of approximately 20 K at 1,000 K . As will be shown later, air temperatures obtained from the Ricardo E6 engine have been determined with a maximum error of approximately 40 K, with a mean standard deviation in the CARS-derived temperature distribution of approximately 40 K. The method retains its accuracy and validity, and is suitable for adoption in rotational and vibrational CARS.

In addition, this paper presents new results for the compression and expansion of air during engine motoring, and a correction to the original results, for the variation in the non-resonant background that occurred in the engine as a result of the reduced nitrogen mole fraction obtained in the unburned fuel-air mixture prior to combustion. We also attempt to estimate the correction necessary for the presence of methanol in the methanol-air mixture in the engine, and its effect on the nitrogen vibrational CARS spectra.

The paper begins with a brief revision of the theoretical basis of the non-linear minimisation of sum of squares of residuals, the derivation of the normalised cross-correlation function, and its Fourier properties, and the extension of the technique to fitting discrete data functions. This is followed by a description of the CARS system, and its use in the High Pressure, High Temperature (HPHT) optical cell for the generation of an experimental database of vibrational CARS spectra. The paper concludes with the description and analysis of CARS temperature measurements in a motored and knocking Ricardo E6 engine.

2. The Normalised Cross-Correlation Function

2.1 Introduction

As stated earlier, conventional gas phase CARS thermometry involves the comparison of a set of many single-shot experimental spectra obtained from a test volume, with a computed library of compatible CARS spectra. The comparison is normally performed using a non-linear least squares technique, often employing Marquardt-Levenberg iteration [38, 43].

Section 2.2 introduces the general problem of minimising the sum of normalised squared differences as a means of quantitatively comparing a test function (an experimental CARS spectral profile) against a set of base functions (the library of computed CARS spectra). The mathematical statement of the problem is then reformulated in terms of the normalised cross-correlation (or cross-covariance) function.

The cross-correlation function is closely related to the Fourier convolution function, and is therefore amenable to Fourier analysis. This facilitates the fast computation of many cross-correlations using dedicated Fast Fourier Transform (FFT) algorithms and/or processors.

2.2 The Normalised Non-Linear Least Squares Method

Given two continuous real functions $f(x)$ and $g(x)$ over the domain of x, the mean square normalised non-linear least squares minimisation criterion is expressed as

$$\alpha_{min}(x') = min\left[\int_{-\infty}^{\infty}\left(\frac{f(x)}{\sqrt{\int_{-\infty}^{\infty} f^2 dx}} - \frac{g(x-x')}{\sqrt{\int_{-\infty}^{\infty} g^2 dx}}\right)^2 dx\right]. \qquad 2.1$$

A shifting variable x' is introduced explicitly into Equation 1.1 to facilitate the optimal overlap of the two functions in the domain. The minimum of $\alpha(x')$ is normally found by Marquardt-Levenberg iteration, which requires robust termination criteria.

A potential problem arises during the minimisation of the sum of mean square differences if one or both of the functions contain data noise. The sum of square differences may lead to many local minima occurring in the neighbourhood of the true minimum. Attempted iteration towards the true minimum can result in a convergent solution at the wrong local minimum.

The principal disadvantage of the normalised non-linear least squares method (iteration to the incorrect minimum) may be addressed by reformulating the non-linear problem into a linear form that is amenable to Fourier analysis, is quickly and easily determined over the entire domain, and provides an objective measure of goodness-of-fit during comparison of data functions.

Expanding the integrand in Equation 1.1 yields the expression

$$\alpha_{min}(x') = min\left[2 - 2\frac{\int_{-\infty}^{\infty} f(x)g(x-x')dx}{\sqrt{\int_{-\infty}^{\infty} f^2 dx \int_{-\infty}^{\infty} g^2 dx}}\right]. \qquad 2.2$$

The minimum of $\alpha(x')$ occurs when the function $\frac{\int_{-\infty}^{\infty} f(x)g(x-x')dx}{\sqrt{\int_{-\infty}^{\infty} f^2 dx \int_{-\infty}^{\infty} g^2 dx}}$ is maximum. This function is just the mean square normalised cross-correlation or normalised cross-covariance function.

The above analysis can be extended to discrete data functions f_j and g_j over the discrete domain of j, $j \in \{1, 2, 3, \ldots, N\}$ The normalised non-linear least squares minimisation criterion is then

$$\alpha_{min}^{k} = min\left[\sum_{j=1}^{N}\left(\frac{f_j}{\sqrt{\sum_{j=1}^{N} {f_j}^2}} - \frac{g_{j-k}}{\sqrt{\sum_{j=1}^{N} {g_j}^2}}\right)^2\right]. \qquad 2.3$$

Expanding the above expression as before, the minimum of α^k occurs when $\frac{\sum_{j=1}^{N} f_j g_{j-k}}{\sqrt{\sum_{j=1}^{N} {f_j}^2 \sum_{j=1}^{N} {g_j}^2}}$ is maximum. This is just the discrete, mean square normalised cross-correlation or cross-covariance function.

2.3 The Cross-Correlation Method of Fitting CARS Spectra

The normalised cross-correlation function $h(x')$ is defined for mean square integrable real functions $f(x)$ and $g(x)$ as

$$h(x') = \frac{\int_{-\infty}^{\infty} f(x)g(x-x')dx}{\sqrt{\int_{-\infty}^{\infty} f^2 dx \int_{-\infty}^{\infty} g^2 dx}}. \qquad 2.4$$

$h(x)$ is closely related to the Fourier convolution function $(f \otimes g)(x)$, which is defined as

$$(f \otimes g)(x') = \int_{-\infty}^{\infty} f(x)g(x'-x)dx. \qquad 2.5$$

Defining the Fourier transform as

$$F(k) = \int_{-\infty}^{\infty} f(x)e^{-ikx}dx, \qquad 2.6$$

and the inverse Fourier transform as

$$f(x) = \frac{1}{2\pi}\int_{-\infty}^{\infty} F(k)e^{ikx}dk, \qquad 2.7$$

then the Fourier transform of the convolution function has the form

$$\mathcal{F}(f \otimes g)(k) = F(k)G(k), \qquad 2.8$$

where $F(k)$ and $G(k)$ are the Fourier transforms of $f(x)$ and $g(x)$ respectively. The Fourier transform of the normalised cross-correlation function has the form

$$\mathcal{F}(h)(k) = H(k) = \frac{-F(k)G^*(k)}{\sqrt{\int_{-\infty}^{\infty} f^2 dx \int_{-\infty}^{\infty} g^2 dx}}. \qquad 2.9$$

The normalised discrete cross-correlation function h_k is defined for discrete real data functions f_j and g_j over the domain of j as

$$h_k = \frac{\sum_{j=1}^{N} f_j g_{j-k}}{\sqrt{\sum_{j=1}^{N} {f_j}^2 \sum_{j=1}^{N} {g_j}^2}} \qquad 2.10$$

This form of the normalised discrete cross-correlation function is very simple to calculate numerically. h_k will have its maximum value when the two mean square normalised functions for f_j and g_j are maximally overlapped. For functions with a single prominent maximum, such as CARS spectra, the numerical calculation can be significantly shortened. Instead of calculating h_k for all possible values of k, one can initially shift g_{j-k} so that its maximum coincides with that of f_j , and then interpolate the maximum of h_k for a limited set of values around this point of coincidence.

Alternatively, h_k can be determined over the entire domain of k through the discrete Fourier transform properties of h_k, i.e.

$$h_k = \frac{-\frac{1}{2\pi}\sum_{n=1}^{N} F_n G_n^* e^{ink}}{\sqrt{\sum_{j=1}^{N} f_j{}^2 \sum_{j=1}^{N} g_j{}^2}}, \qquad 2.11$$

where F_n and G_n are the discrete Fourier transforms of f_j and g_j respectively, and $i = \sqrt{-1}$.

Therefore the minimisation of the mean square normalised sum of squares of differences is transformed to a simpler, linear and more systematic method of maximising normalised cross-correlations. The determination of the global maximum value of the normalised cross-correlation is elementary, and is a consequence of the mean square integrability and the linear product of the test functions..

The application of the cross-correlation method for fitting nitrogen Q-branch CARS spectra begins with the analysis of the spectra in the frequency domain. The discrete real data functions F_n and G_n are real CARS spectra obtained from an unknown combustion environment and a CARS spectral database respectively.

The discrete mean square normalised cross-correlation function for the CARS spectra in the frequency domain is defined to be

$$H_k = \frac{\sum_{j=1}^{N} F_j G_{j-k}}{\sqrt{\sum_{j=1}^{N} F_j{}^2 \sum_{j=1}^{N} G_j{}^2}}. \qquad 2.12$$

The Fourier transform properties of the discrete normalised cross-correlation function means that H_k can also be expressed as

$$H_k = \frac{-\frac{1}{2\pi}\sum_{j=1}^{N} f_j g_j^* e^{-ijk}}{\sqrt{\sum_{j=1}^{N} F_j{}^2 \sum_{j=1}^{N} G_j{}^2}}, \qquad 2.13$$

where $f_j = \sum_{k=1}^{N} F_k e^{ijk}$ and $g_j = \sum_{k=1}^{N} G_k e^{ijk}$ respectively. The subscript j in f_j and g_j refers to discrete successive instants in the time domain.

2.4 Comparison of the Cross-Correlation with the Minimisation of Sum of Squared Differences

It was shown earlier (Section 2.2) that the cross-correlation method is mathematically equivalent to the minimisation of sum of square differences method, and was derived from it. However, there are two fundamental differences between the two methods that distinguish them from each other. The first distinction is obtained in the useful Fourier properties of the cross-correlation function, which is not shared with the mathematical form of the sum of squared differences. The use of Fast Fourier Transform software and/or hardware facilitates the fast computation of many cross-correlations.

The second distinction between the two methods is found in the manner in which the global extremum is obtained. The minimum of the sum of squared differences is obtained by iteration. Various iterative algorithms are in use, but the Marquardt-Levenberg (ML) iterative method (damped least squares (DLS) method) is the most popular. However, the ML iterative algorithm suffers from two disadvantages. The first disadvantage occurs when the discrete experimental data contains significant data noise. In this case, the normalised sum of squared differences may exhibit many local minima in the neighbourhood of the global minimum. Finding the global minimum may involve repeated checks of the minima associated with the initial guess in order to ensure that the true global minimum has been obtained.

The second disadvantage of the Marquardt-Levenberg iterative method is that convergence to the global minimum may be slow if the multi-variable surface in the neighbourhood of the minimum is gently curving with a large local radius of curvature. In this case, the method will find the global minimum correctly, but the algorithm may be relatively slow to find the minimum.

By contrast, the discrete normalised cross-correlation function can be quickly calculated numerically over the entire domain using Fourier techniques (due to its advantageous Fourier properties), or in the neighbourhood of the maximum by direct calculation. The remainder of the problem then lies in finding where in the domain the global maximum occurs, and the global maximum value.

A disadvantageous property of the discrete, normalised cross-correlation function which is shared with the minimisation of sum of square differences, has been discovered during this analysis. The discrete, normalised cross-correlation function is a shifted, normalised inner product, which obtains the correct global maximum value in most cases. However, if the spectral data is noisy, many local maxima may occur in the neighbourhood of the global maximum. This is the corollary of the many local minima that may occur in the neighbourhood of the global minimum in the sum of squared differences method. It then becomes difficult to fit a polynomial to the discrete cross-correlation values in the neighbourhood of the global maximum in order to find the interpolated global maximum. Indeed, if the spectral data is too noisy, than the discrete cross-correlation function may produce an incorrect global maximum as a result of the simultaneous effect of correlating the spectra, together with shifting the spectra in the domain.

3. The CARS System

The CARS system employed in this study consisted of a pulsed, passively Q-switched Nd:YAG laser with internal etalons, producing TEM00 laser emission at 532 nm, of approximately 13 ns duration. The Nd:YAG laser was aligned to operate at 1 Hz to 10 Hz pulse frequency, producing laser light with a pulse energy of approximately 180 mJ at 532 nm. Approximately 30 % of the Nd:YAG laser emission was separated from the main beam using a laser beam splitter, and employed to pump an amplified broad-band dye laser (using Rhodamine 6G in ethanol). The dye laser emission was selected in order for the pump frequency minus the dye laser frequency to resonantly excite the first vibrational state of molecular nitrogen ($\Delta\varepsilon_{vib} = \hbar(\omega_P - \omega_S)$). The 532 nm pump beam and the 607 nm Stokes beam normally left the optical table with a pulse energy of approximately 120 mJ and 5 mJ respectively.

The CARS optical table contained a beam splitter and an adjustable dichroic mirror that could be employed to overlay the pump and Stokes laser beams co-incidently in order to achieve a co-linear CARS configuration, or to split and separate the beams in order to produce a planar BOXCARS beam configuration. Following the generation of the nitrogen CARS signal in the interrogation volume, the pump and Stokes beams were separated from the CARS signal using a low pass dichroic mirror (reflective

above 500 nm, transmissive below 500 nm). The pump and Stokes beams were then re-directed into an optically accessible high pressure Argon gas cell in order to generate a simultaneous non-resonant reference CARS signal.

There has been considerable analysis of suitable referencing methods over the years. Single-shot resonant CARS spectra are proportional to the square of the spectral radiation flux of the pump beam, and linear in the spectral radiation flux of the Stokes beam. The use of a multi-mode pump beam, and mode competition in the Stokes beam are likely to produce very noisy single-shot resonant and non-resonant spectra. This can lead to noisy referenced single-shot spectra. In this case, it is often better to normalise the single shot resonant spectra with a mean non-resonant spectrum. However, when resonant and non-resonant CARS spectra are generated simultaneously using a TEM00 pump laser, the spectra are much more stable on a shot-to-shot basis, and simultaneous referencing reduces the effect of Stokes laser mode competition, and properly normalises the resonant CARS spectra [4, 25].

The resonant and non-resonant reference CARS signals were then directed at different heights through a 45^{o} angled slit into a CARS spectrometer employing a 2,100 line/cm Jobin-Yvon holographic grating and 2x optical telescope to direct the test and reference CARS spectral profiles onto a gated, intensified 16-bit, 1024-channel EG&G 1461 diode array detector. The CARS spectrometer produced a dispersion of 0.287 cm^{-1} per pixel (0.00643 nm/pixel) at 473.34 nm (wavelength for 532nm pumped nitrogen Q-branch CARS). The simultaneous resonant and non-resonant reference CARS signals were directed onto two 256 pixel wide sections separated by a 512 pixel wide centre section on the 1024-channel detector, producing two spectrometer detector widths of 73.97 cm^{-1} (1.646 nm) each.

In order to account for the varying sensitivity across the intensified diode array, the spectrometer grating position was adjusted in order that the maxima of the resonant CARS spectral profiles obtained from ambient air were located at the same pixel value for all of the HPHT cell and engine experiments. The corresponding position of the non-resonant reference spectra was determined by fine adjustment of the position that the non-resonant CARS reference signal entered the spectrometer via the angled slit. This systematic alignment of the resonant and non-resonant spectra over the

same pixel range on the intensified detector facilitated a consistent comparison of ratioed spectra.

In the years following these experiments, Ewart *et al*. [28] demonstrated that the use of a modeless dye laser was able to reduce, or even eliminate the effect of dye laser mode competition during the generation of experimental CARS spectra, which resulted in improved measurement precision [29]. Nevertheless, the CARS system described here remained capable of producing distributions of referenced database spectra in the High Pressure High Temperature (HPHT) cell with standard deviations of 20 K to 35 K in the 400 K to 700 K temperature range, and 30 K to 45 K in the 700 K to 1,100 K temperature range, for all pressures in the 1.0 bar to 21.0 bar range.

4. The High-Pressure High-Temperature (HPHT) Cell Experiment

4.1 Motivation and Objectives

The high-pressure high-temperature (HPHT) optical cell was designed and built in order to generate experimental CARS spectral databases with different vapour mixtures, in order to calibrate pressure narrowing effects in the computational determination of CARS spectra at high pressure. At the time of the CARS experiments in the engine, the collision models for nitrogen in the presence of other gas species were unreliable and inaccurate for the computation of database spectra for the temperatures and pressures obtained in engines. Consequently, it was thought that the generation of an experimental CARS spectral database covering the range of temperatures and pressures in an engine would facilitate the accurate determination of in-cylinder engine temperatures.

This led to the design and development of the High Pressure, High Temperature (HPHT) optically accessible cell, which would be employed for the generation of the experimental database of nitrogen CARS spectra, appropriate for the temperatures and pressures achieved in the engine. It was thought that the experimental spectra obtained from the HPHT cell could be used to determine in-cylinder engine temperatures directly, as the same CARS system (pump and Stokes lasers, and CARS

spectrometer and detector) was being employed for CARS signal generation and detection in both applications.

4.2 The High-Pressure High-Temperature (HPHT) Optical Cell

The HPHT cell consisted of two hollow concentric stainless steel cylinders of different radii, one held in place inside the other with thermal insulation fitted around the inner cylinder. A ceramic frame fitted to the inside of the inner cylinder contained four thin cylindrical, helically wound nichrome heating elements, placed along evenly spaced axial grooves cut into the inner face of the ceramic frame. The outer cylinder was pressure sealed, designed to hold gas pressures ranging from atmospheric pressure to 20 bar gauge pressure. Figure 1 is a simplified schematic that illustrates the design and layout of the HPHT cell.

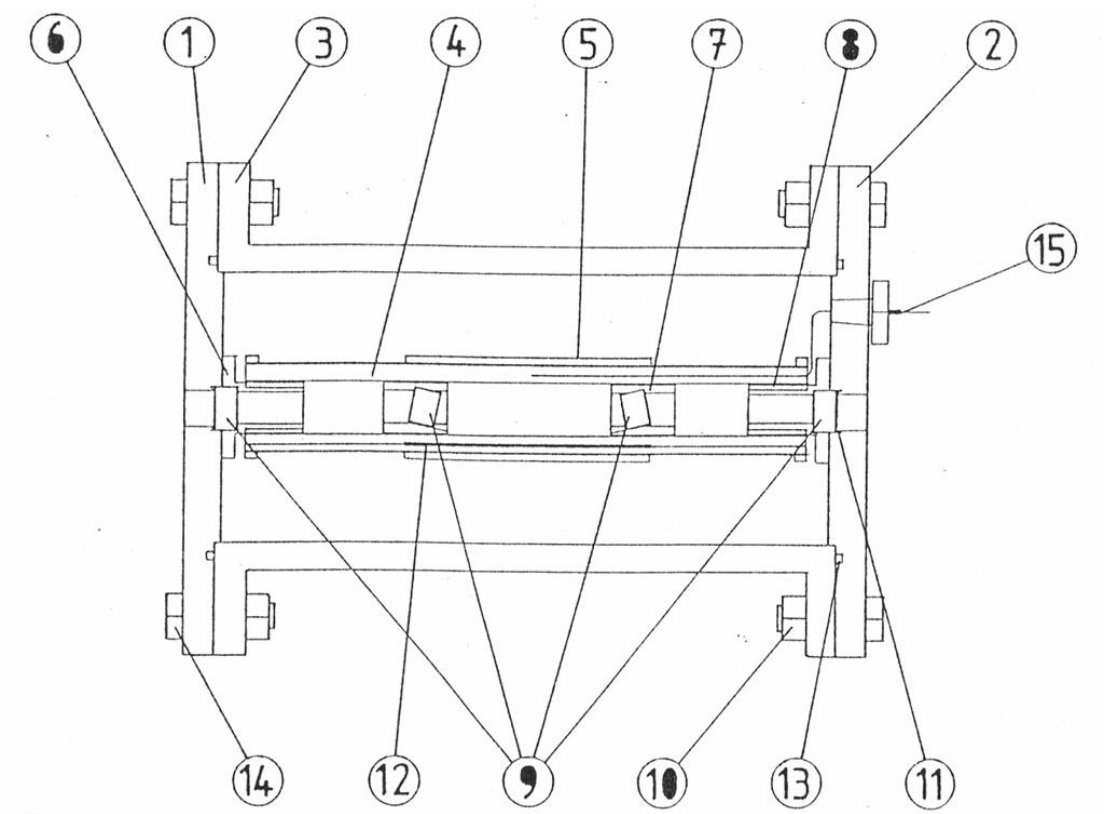

Number	Item Name	Material
1	End Plate L/Hand	St. Steel 316
2	End Plate R/hand	St. Steel 316
3	Pressure Cell	St. Steel 316
4	Ceramic Tube	Ceramic
5	Ceramic Tube Holder	St. Steel 316
6	Outer Window Holder	St. Steel 316
7	Inner Window Holder	St. Steel 316
8	Insulator	
9	Windows	Quartz glass
10	M16 Nut	Mild Steel
11	O-Ring	Silicone
12	Heater Element	Nichrome
13	O-Ring	Neoprene
14	M16 Bolt	Mild Steel
15	Thermocouple	Nichrome St. Steel 316

Figure 1: Schematic of High Pressure High Temperature Cell

The temperature in the HPHT cell was steadily maintained using a type K control thermocouple connected to a commercial temperature control system, and placed along the inside wall centrally along the axis of the ceramic frame. Two measurement type K thermocouples were placed along the central axis and along the central radius, in order to monitor the interior temperature of the HPHT cell.

The cell was designed for temperatures ranging from ambient (~ 285 K) to 1300 K, and pressures ranging from ambient atmospheric pressure to 20 bar gauge pressure. The experimental uncertainty in the cell pressure was determined to be ± 5 kPa, while the uncertainty in the thermocouple measurements of temperature were ± 3 K. Table 1 shows measured temperatures for a number of high temperature and high pressure conditions in the cell. The control thermocouple measured a local temperature adjacent to the ceramic surface that was systematically 15 K to 20 K higher than the two measurement thermocouples. The measurement thermocouples were able to determine the local temperature in the CARS measurement region with an experimental uncertainty of ± 10 K over the entire operating range of the HPHT cell.

Table 1: Thermocouple Calibration Measurements of Temperature in the High Pressure, High Temperature Cell

Gauge Pressure (bar)	*Control Temperature (K)*	*Axial Thermocouple Temperature (K)*	*Radial Thermocouple Temperature (K)*
5.0	346	334	320
5.0	707	694	690
10.0	499	478	464
10.0	709	703	688
15.0	601	579	570
15.0	700	682	658
15.0	710	690	678
20.0	802	784	782

The HPHT cell was employed to generate a database of referenced BOXCARS nitrogen Q-branch spectra obtained in air. Five sets of fifty single shot and simultaneous reference nitrogen CARS spectra were obtained from the HPHT cell for the selected conditions. Mean processed, referenced spectra were obtained for each condition by firstly, dividing the single shot resonant spectra by their corresponding non-resonant spectra, and secondly, finding the mean referenced spectra from the five sets of fifty referenced single shot spectra. Table 2 shows the range of HPHT cell temperatures and pressures employed during the generation of the database.

At each pressure, one of the five sets of fifty spectra corresponding to the middle temperature within each temperature range specified in Table 2, was compared with the mean spectra forming the experimental database. This comparison showed that the attainable single-shot precision at each pressure varied from 20 K to 35 K at the lower range of temperatures and pressures (280 K to 650 K, 1 bar to 5 bar), and from 30 K to 45 K at the higher range of temperatures and pressures (500 K to 1,200 K, 6 bar to 18 bar), a result of shot-to-shot variability of the CARS spectra, due to dye laser mode competition [43]. An example of this analysis is presented later in Section 4.4.

Table 2: Selected Temperature Range as a Function of Pressure for the Experimental CARS Database

Pressure (bar)	*Temperature Range (K)*	*Interval (K)*
1.0	293 – 548	23
1.5	323 – 548	25
2.0	348 – 548	25
2.5	373 – 573	25
3.0	379 – 571	24
3.5	423 – 623	25
4.0	431 – 623	24
4.5	473 – 673	25
5.0	473 – 698	25
5.5	473 – 723	25
6.0	498 – 748	25
6.5	523 – 773	25
7.0	573 – 798	25
7.5	573 – 823	25
8.0	673 – 858	25
8.5	623 – 823	25
9.5	498 – 873	25
11.0	643 – 963	40
12.5	723 – 1003	40
14.0	763 – 1003	40
15.0	763 – 1003	40
16.0	763 – 1043	40
18.0	803 – 1083	40

4.3 Alignment and Focussing in the Spectrometer

When CARS experiments are performed, the optical alignment is always a delicate procedure. The final test of optimal alignment is the quality of the focussed Nd:YAG oscillator signal and CARS signal on the detector, in this case an intensified diode array. Every experiment usually requires a new alignment of the optics, and often optical alignment needs to be repeated daily for the same experiment.

Repeated alignment during the course of a CARS experiment can result in subtle changes to the focussing of the CARS signal onto the optical detector. This means that spectra obtained under the same physical conditions at different times and

containing the same spectral information, may appear slightly different. This is because the alignment and the focussing of the CARS signal onto the detector is marginally different.

Focussing of CARS spectra onto a detector is usually taken into account numerically using an instrument function. The instrument function is usually modelled by a Voigt function in the frequency domain, and different focussing conditions should be reflected in the shape of the employed Voigt profile.

In order to compare the spectral information contained in two spectra obtained under the same conditions, but with different focussing, required an empirical matching of the instrument functions. This was performed by broadening or narrowing one of the spectra using a Gaussian profile in the time domain until the global maximum value of the cross-correlation coefficient was obtained [37].

4.4 HPHT Cell Data Analysis: Fitting of Experimental Spectra

In order to assess the advantages of fitting experimental spectra using the cross-correlation method, and determine the accuracy and experimental uncertainty associated with the empirical methodology outlined earlier, a number of cross-correlation validation tests were conducted at various HPHT cell temperatures and pressures. The test data were obtained on a different day to the database images. In order to make the comparison realistic, the CARS system was re-aligned between the development of the CARS spectral database, and the later temperature test data.

Two examples of the cross-correlation validation tests conducted in the HPHT cell are included here. Figure 2 shows a histogram presenting the distribution of single-shot temperatures deduced from one set (one out of five for each condition) of 50 single shot CARS temperature measurements obtained in the HPHT cell, using the normalised cross-correlation method, together with the deduced mean temperature, sample standard deviation, and standard deviation of the mean. The data presented in Figure 2 refers to the HPHT cell temperature and absolute pressure set at 673 K ± 10 K, and 7.0 bar ± 0.05 bar respectively.

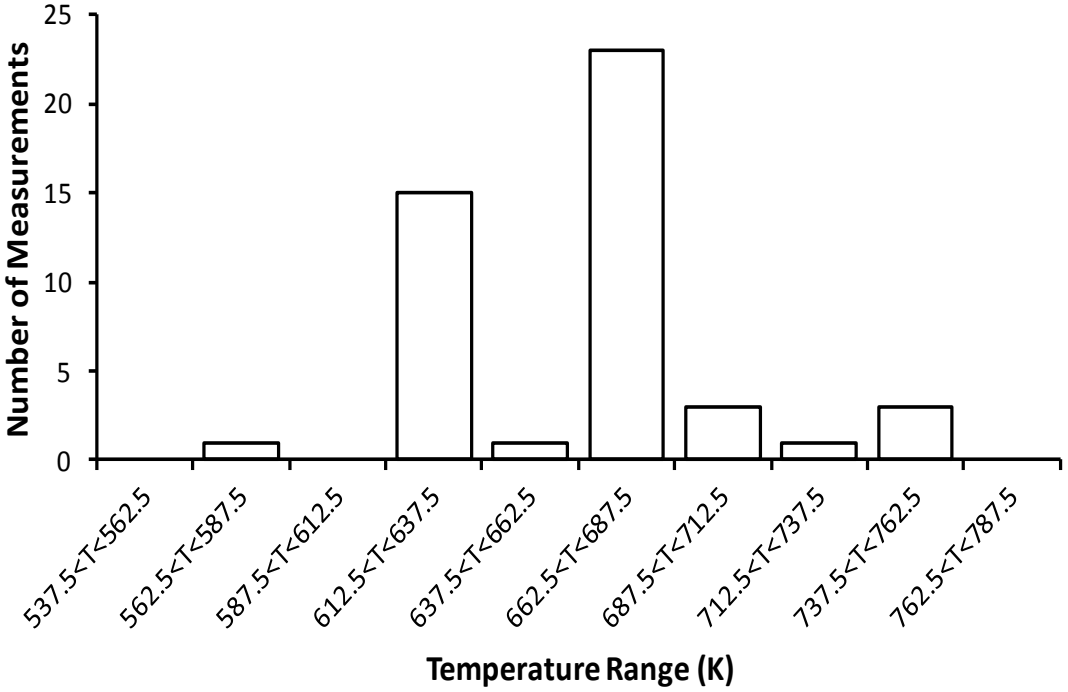

Figure 2: Distribution of 47 Single-shot CARS Temperature Measurements obtained in the HPHT Cell using Cross-correlation Analysis, (T_{cell} = 673 K ± 10 K, P_{cell} = 7.0 bar ± 0.05 bar, T_{CARS} = 664 K ± 36 K (σ_{CARS}), T_{meas} = 664 K ± 10 K ($2\sigma_{mean}$)).

The second example of the cross-correlation validation is shown in Figure 3, which is a graph of the correlation coefficient as a function of temperature, obtained in the HPHT cell. The graph was obtained by correlating two mean spectra obtained at a specified temperature and pressure (983 K, 15.0 bar), with mean spectra comprising the 15.0 bar database (783 K ± 10 K to 1023 K ± 10 K at 40 K intervals). The maximum cross-correlation was achieved against the database spectra at 983 K (as expected). A polynomial best fit to the cross-correlation data suggested that the maximum cross-correlation was attained at 967 K for both of the mean spectra obtained from the two samples. These two mean CARS spectra therefore produced an absolute and relative uncertainty in the measured CARS temperature of - 16 K and 0.017 (1.7 %) respectively, at an HPHT cell temperature and pressure of 983 K and 15.0 bar.

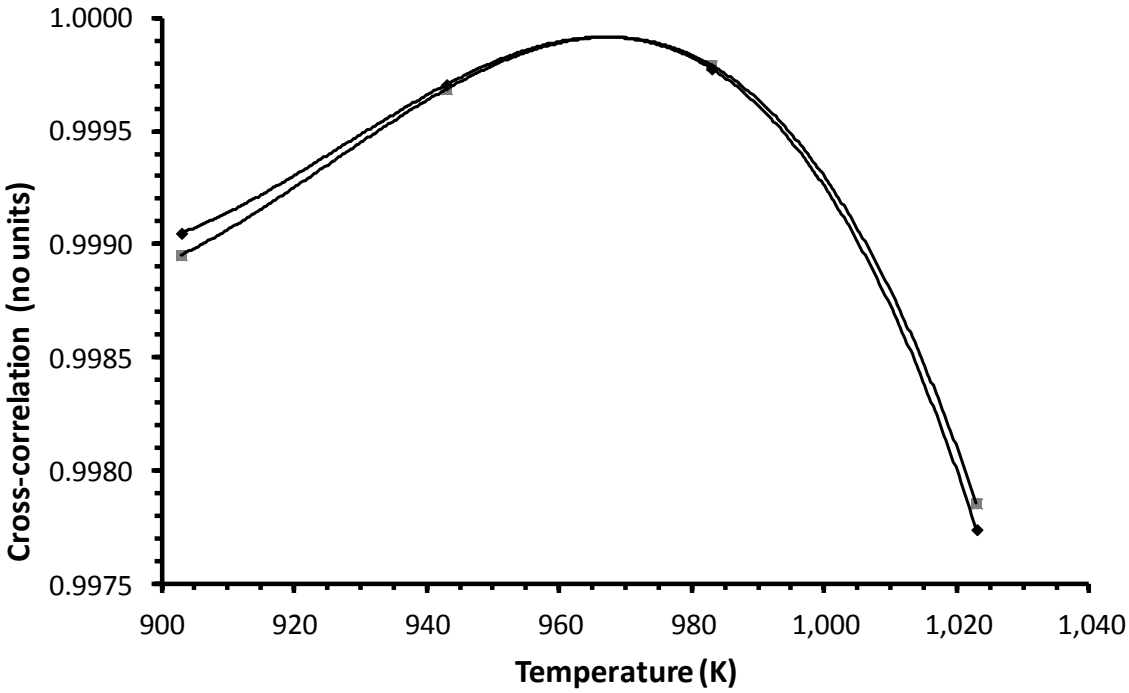

Figure 3: Maximum Cross-Correlation as a Function of Temperature Obtained in the HPHT Cell for Two Mean CARS Spectra (983 K, 15.0 bar).

Finally, a sample of 45 mean CARS spectra obtained from the HPHT cell at various temperatures and pressures were compared with the database reference spectra obtained at the same pressure, in order to determine the absolute and relative uncertainty in the CARS mean temperature measurements. Figures 4 (a) and (b) show the absolute and relative uncertainties in the CARS mean temperature measurements obtained in the HPHT cell.

4.5 HPHT Cell Results and Discussion

Figure 2 shows the histogram associated with one of the five sets of fifty single shot CARS spectra, obtained in the HPHT cell at a preset temperature and pressure of 673 K ± 10 K and 7.0 bar ± 0.05 bar respectively. The histogram temperatures were obtained by finding the temperature corresponding to the maximum cross-correlation of the referenced single-shot spectra against the experimental database spectra. The histogram shown in Figure 2 suggested a mean temperature of 664 K, together with a standard deviation of 36 K. 27 out of the 47 single-shot spectra (57.4 %) comprising the sample had predicted temperatures within 25 K of the mean.

Three single-shot temperatures were missing from the temperature histogram shown in Figure 2. This was because the two intra-cavity etalons in the Nd:YAG laser oscillator cavity produced TEM00 radiation at 532 nm for 95 % of emitted laser pulses. Small variations in the temperature of the laser table resulted in multi-mode operation for approximately 5% of pulses. These multi-mode laser pulses subsequently produced CARS spectra that could not be fitted to the database spectra. In this case, three of the fifty single-shot spectra were produced from the Nd:YAG laser operating multi-mode, were unable to be fitted to the mean spectra comprising the CARS database.

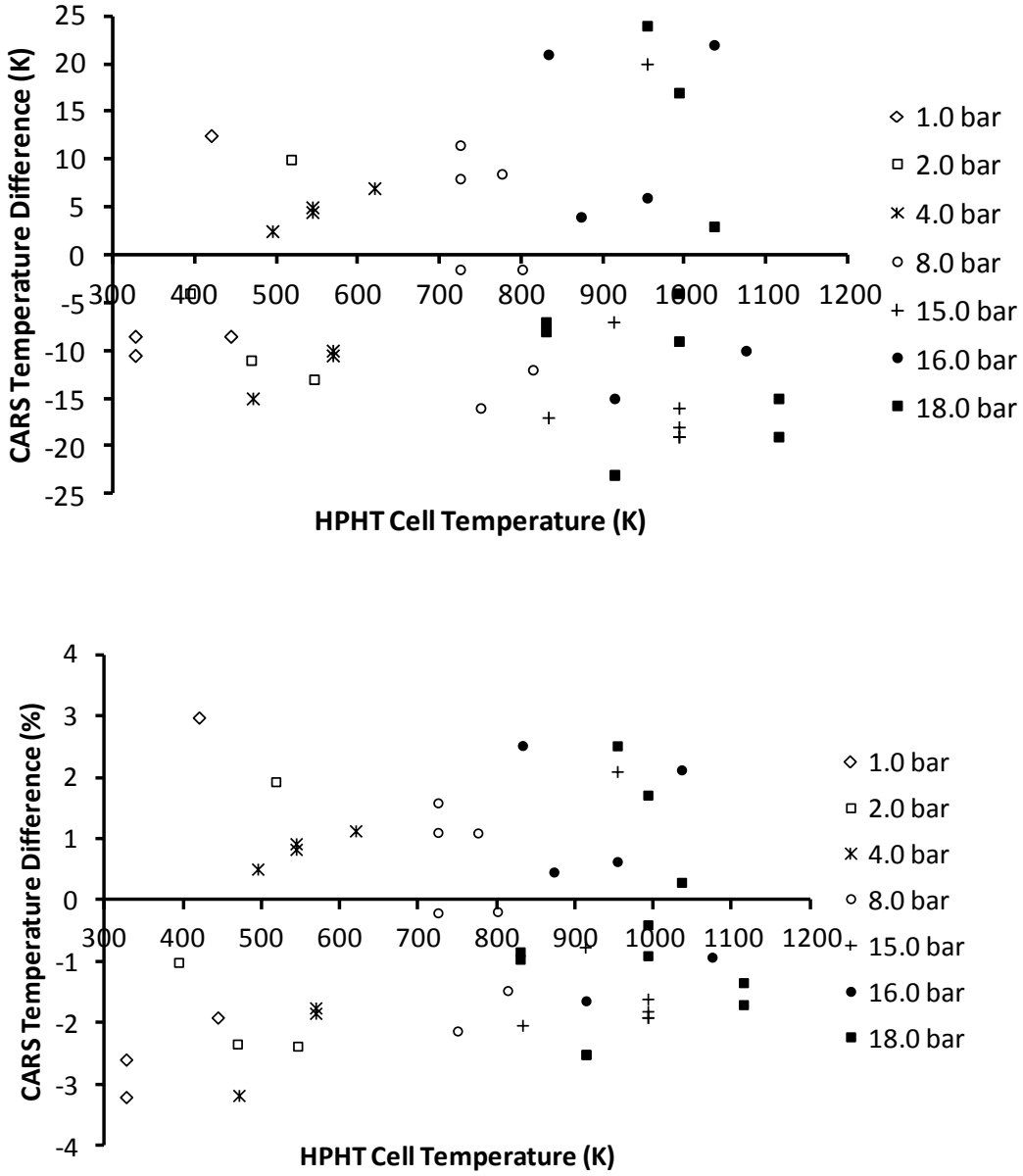

Figure 4: Absolute and Relative Uncertainty in CARS Mean Temperature Measurement as a Function of HPHT Cell Temperature (K).

The graphs presented in Figures 4 (a) and (b) suggests that the cross-correlation method of spectral fitting, coupled to the experimental CARS spectral database, was capable of determining temperature in the HPHT cell with an absolute uncertainty of ± 15 K for 1.0 bar to 10.0 bar cell pressure (3 % relative uncertainty at 300 K, 1.0 bar, reducing down to 2 % relative uncertainty at 800 K, 10.0 bar), and an absolute uncertainty of ± 24 K for 11.0 bar to 18.0 bar cell pressure (~ 2.5 % relative uncertainty over the temperature range 800 K to 1,150 K).

An analysis of the behaviour of the experimental CARS spectra as a function of pressure revealed that the spectra were subjected to a non-linear pressure narrowing rate in the 5.0 bar to 10.0 bar range. The pressure narrowing of the nitrogen CARS spectra can be observed in Figure 5, which shows four CARS spectra obtained at a common temperature of 723 K, and pressures 5.5 bar, 7.5 bar, 9.5 bar and 11.0 bar respectively. The normalised CARS signal intensities are plotted on a logarithmic scale, presented as a function of the CARS frequency (cm^{-1}).

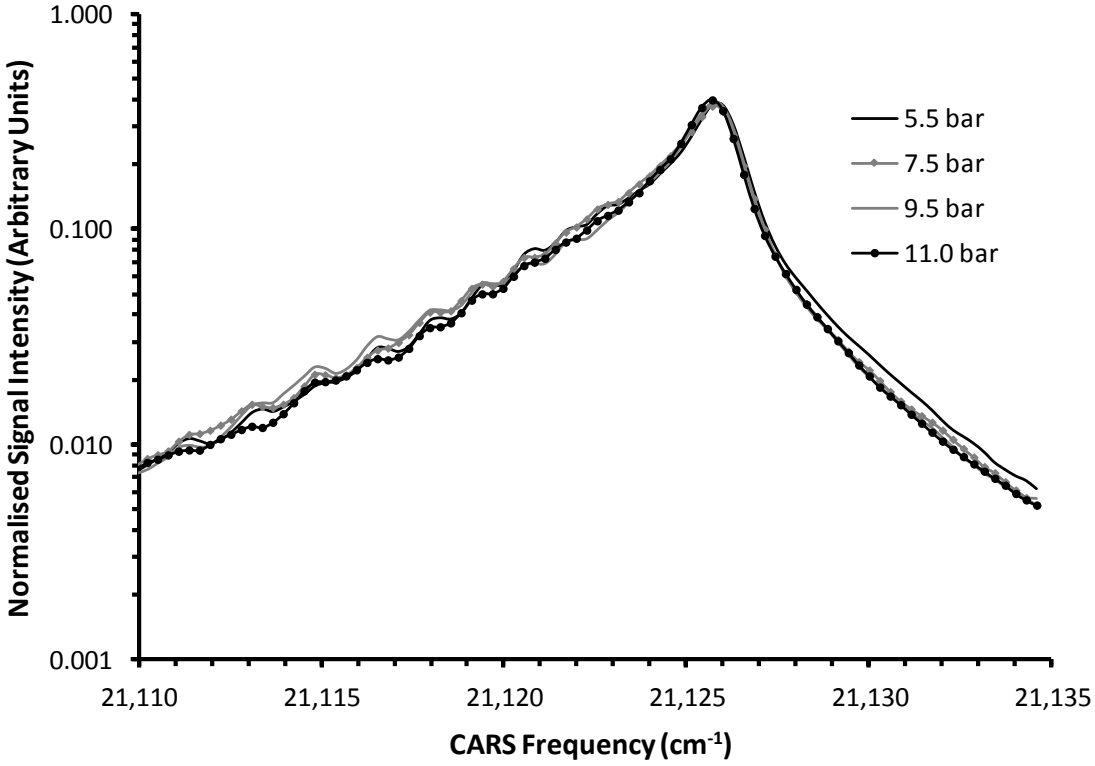

Figure 5: Mean CARS Spectra obtained in the HPHT Cell at 723 K, for Various Pressures (5.5 bar, 7.5 bar, 9.5 bar, 11.0 bar).

The mean CARS spectra shown in Figure 5 reveal that the full width at half maximum (FWHM) remained almost unchanged at 2.727 cm^{-1} ± 0.143 cm^{-1} for a doubling of the pressure from 5.5 bar to 11.0 bar. However, the full width of the central region, together with the central-left region showing the rotational line structure (21,120 cm^{-1} to 21,125 cm^{-1}) was subjected to significant narrowing over the pressure range 5.5 bar to 9.5 bar. The 11.0 bar spectral signal remained very similar to the 9.5 bar signal. These two observations, taken together, reveal that CARS spectra were subjected to a significant pressure narrowing rate in the pressure range 5.0 bar to 9.5 bar, followed by a significantly reduced rate above 9.5 bar. The conventional spectral scaling law (Modified Exponential Gap (MEG) Law [5]) that was used to calculate pressure narrowing effects was unable to capture the precise rate of pressure narrowing in this pressure range, together with the decrease in the pressure narrowing rate above 10 bar. This resulted in a small variation in the accuracy of the modelled CARS spectra in this range of pressures.

5. Application to a High Temperature, High Pressure Environment: Temperature Measurements in a Spark Ignition Engine

The experimental spectra obtained from the HPHT cell were employed to determine the mean temperature profile occurring during the compression stroke and expansion stroke in a motored Ricardo E6 research engine. This was followed by measurements of the fuel-air mixture temperatures occurring during the compression stroke in a knocking Ricardo E6 engine, using coal-to-liquid (CTL) gasoline and methanol as engine fuels.

5.1 Experimental Configuration

5.1.1 The Optically Accessible Ricardo E6 Engine

The Ricardo E6 research engine employed in this project was a single cylinder variable compression ratio research engine equipped with a Lawrence Scott dynamometer. The combustion chamber was cylindrical in shape, the piston crown and cylinder head being flat. The Ricardo E6 in-cylinder geometry facilitated a low-

swirl, low-turbulence intake air-flow. The engine was operated with a bore, stroke and connecting rod length of 75 mm, 111 mm, and 242 mm respectively.

The engine was fitted with a 12 mm high spacer, located between the cylinder head and the engine block. The spacer housed two diametrically opposed, 8mm diameter, Spectrosil-B uv grade fused silica windows in order to provide optical access to the cylinder. With the spacer in position, the maximum obtainable engine compression ratio was 9.5. The engine was naturally aspirated, and included provision for preheating the air prior to admission to the carburettor. An AVL water-cooled pressure transducer, type 12QP, was used for pressure measurement.

The engine control system employed a crankshaft encoder, which provided a TTL pulse at a pre-determined crankshaft angle. The crankshaft encoder was manually set to provide a TTL pulse at TDC at the beginning of the intake stroke. The TDC pulse was employed to trigger a delayed pulse to fire the Nd:YAG laser, and trigger the intensified diode array. The engine speed was controlled by the dynamometer manually. The variation in the engine speed during the engine tests was ± 10 rpm.

5.1.2 Alignment of the CARS System

The CARS laser tabletop, spectrometer and control computers were re-located to the engine laboratory, and placed on vibration-damped tables. The 8 mm diameter 532 nm TEM00 Nd:YAG pump and 607 nm Stokes dye laser beams were aligned to operate in a co-linear configuration with parallel polarisations. The beams were passed through a 300 mm focal length achromat lens that was mounted 150 mm from the mid-point of the engine block. The focussed beams then passed through the fused silica inlet window of the engine, and were brought to a focal waist at the midpoint of the cylinder 6 mm below the cylinder head. As the beam alignment and focus resulted in a 2 mm diameter beam at the windows, the laser had to be operated at reduced pulse energy in order to avoid optical damage to the windows. It was nevertheless possible to obtain ambient in-cylinder nitrogen CARS peak signal strengths of the order of ten to twenty thousand counts per pixel, providing a single-shot signal-to-noise ratio of approximately 500 – 1000 (9 - 10 bits of real dynamic range).

The 473 nm nitrogen CARS signal, together with the pump and Stokes beams, exited the engine through the outlet fused silica window. The beams were then re-collimated by passing them through a second 300 mm focal length achromat, mounted 150 mm from the centre of the cylinder block on the beam exit side, and then re-directed towards the spectrometer table. Once the co-linear beams had entered the detection optics box containing the spectrometer, detector and reference cell system, a dichroic mirror was employed to separate the 473 nm CARS signal from the pump and Stokes beams. The 473 nm CARS signal was then directed into the spectrometer, while the pump and Stokes beams were directed towards the reference cell containing high pressure Argon.

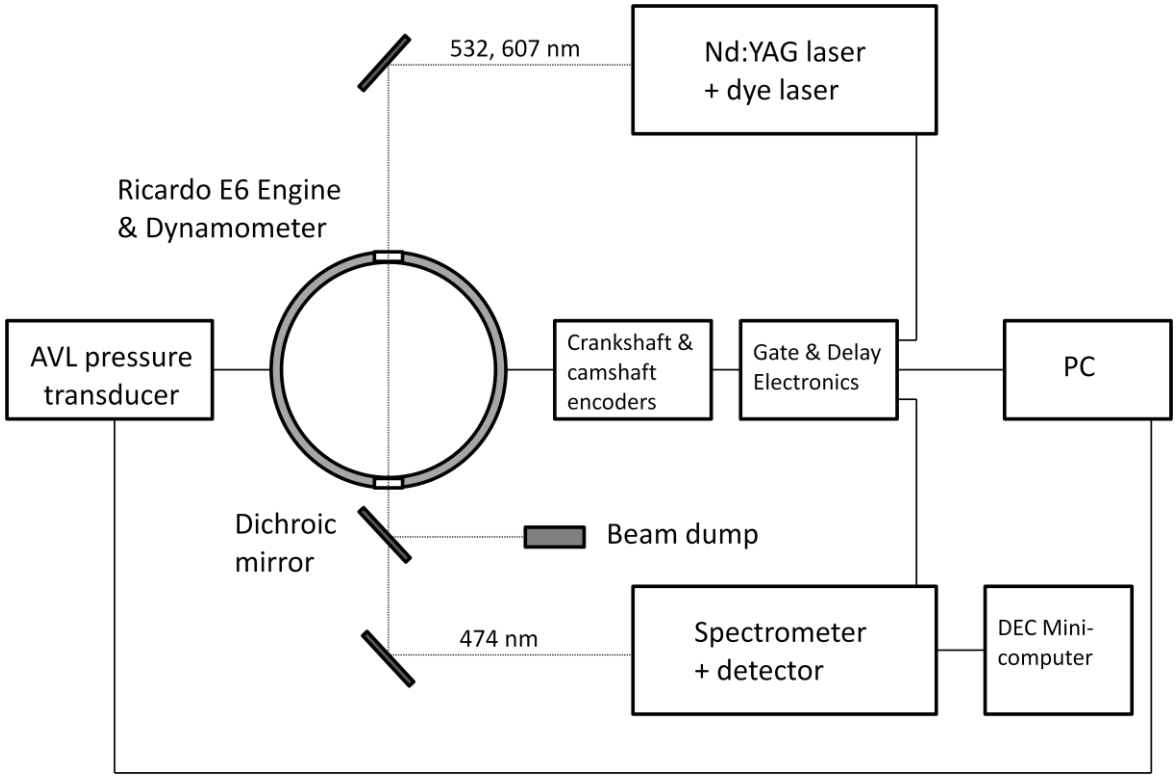

Figure 6: Experimental Layout of CARS System and Ricardo E6 Engine

In order to maintain the consistency of the detector response, the resonant CARS signal and the non-resonant reference signal were aligned to the same 256 pixel wide sections of the detector, separated by a 512 pixel wide central region, consistent with what was described earlier in Section 3. This meant that fitting the referenced engine

spectra against the referenced database spectra was independent of the spatial variation in detector response. For ease and convenience, the CARS spectra obtained from the engine were referenced using mean non-resonant reference spectra, which were obtained from the high pressure Argon reference cell following each engine test.

Figure 6 shows a simple schematic of the diagnostic layout in relation to the engine. Different blocks show the engine control system, the crankshaft and camshaft encoders, the pressure transducer, the timing control, the CARS laser system, and the CARS signal detection system.

5.1.3 Engine Operating Conditions

Table 3 shows the engine operating conditions that were subjected to investigation, the selected crankshaft angles, and the fuels employed during the tests.

The engine was initially motored at 1,000 rpm, with the inlet air preheated to 443 K ± 3 K. Five groups of thirty single shot CARS spectra were obtained at various crankshaft angles during the compression and expansion stroke (identified in Table 3).

This was followed by skip-firing the engine at 1,200 rpm and 1,400 rpm under knocking conditions, using methanol as the engine fuel. Regular engine knock was achieved by preheating the inlet air to 426 K ± 3 K for 1,200 rpm engine speed, and 414 K ± 3 K for 1,400 rpm engine speed, and firing the spark plug at 34^{o} before TDC. Under these conditions, knock occurred at the end of almost every firing cycle. The mean cycle-to-cycle knock intensity was reduced by adjusting the ignition timing, the inlet air temperature, and the fuelling to the engine.

Five groups of thirty single-shot CARS spectra were obtained at various preset crankshaft angles during the compression stroke of the knocking cycles (identified in Table 3). The engine was skip-fired in order to eliminate the effect of residual gas on the following cycle temperature profile and onset of auto-ignition.

Table 3: Ricardo E6 Engine Operating Conditions

Fuel	***Intake Air Temperature (K)***	***Engine Speed (rpm)***	***Crankshaft Angle for Temperature Measurement (degrees before TDC)***
None (motored engine)	443 ± 5	1,000 ± 10	149.5 ± 2.1 89.5 ± 2.7 53.5 ± 3.1 23.5 ± 3.4 0.0 ± 3.6 23.5 ± 3.9 after TDC 53.5 ± 4.2 after TDC
Coal-to-liquid (CTL) gasoline	343 ± 5	1,000 ± 10	179.5 ± 1.8 149.5 ± 2.1 119.5 ± 2.4 101.5 ± 2.6 89.5 ± 2.7 77.5 ± 2.8 65.5 ± 2.9 53.5 ± 3.1 41.5 ± 3.2 29.5 ± 3.3 23.5 ± 3.4
Methanol	443 ± 5	1,200 ± 10	179.5 ± 1.8 150.5 ± 2.1 122.0 ± 2.4 100.0 ± 2.6 89.5 ± 2.7 79.0 ± 2.8 68.0 ± 2.9 57.0 ± 3.1 46.0 ± 3.2 29.5 ± 3.3 23.5 ± 3.4
Methanol	443 ± 5	1,400 ± 10	179.0 ± 1.8 149.0 ± 2.0 120.0 ± 2.2 90.5 ± 2.4 74.0 ± 2.6 57.0 ± 2.8 48.5 ± 2.9 40.0 ± 3.0 31.5 ± 3.1

The methanol knock experiment was followed by operating the engine skip-fired under knocking conditions at 1,000 rpm, using coal-to-liquid (CTL) gasoline. The inlet air temperature was reduced to 353 K, in order to achieve weak knock intensity during most firing cycles. The spark advance was maintained at 34^{o} before TDC. Once again, five groups of thirty single-shot CARS spectra were obtained from the in-cylinder mixture at pre-specified crankshaft angles during the compression stroke in the firing engine (identified in Table 3).

Off-resonance reference spectra were obtained from the optically accessible high pressure Argon gas cell following the CARS data collection from each of the engine tests in order to reduce the effect of single-shot differential mode excitation in the broad-band dye laser.

5.2 Data Analysis: Matching Instrument Functions

As stated earlier, CARS signal alignment onto the spectrometer detector may vary from experiment to experiment, which affects the instrument function from experiment to experiment. The vibrational N_2 CARS signal obtained from ambient air inside the engine at 292 K was compared with the vibrational N_2 CARS signal obtained from inside the HPHT cell at 293 K. These signals were found to exhibit slightly different spectral widths. The spectral width (FWHM) obtained from the HPHT cell was narrower than that obtained from the engine by about 0.43 cm^{-1} at the CARS frequency of 21,126 cm^{-1} (473.35 nm). The mean nitrogen CARS spectra obtained from the HPHT cell and the engine at ambient conditions are shown in Figure 7 (a).

The mean CARS spectrum from the HPHT cell was broadened using a Gaussian function in order to match the spectral width of the mean spectrum obtained from inside the engine. The optimal broadening parameter improved the cross-correlation coefficient for the two mean spectra from 0.9864 to 0.9961. The broadened mean spectrum from the HPHT cell is shown together with the corresponding mean spectrum from the engine in Figure 7 (b). Once the optimal Gaussian broadening parameter had been established, the entire database of CARS spectra obtained from

the HPHT cell was broadened, in order to match the effective instrument functions for the two experiments [37].

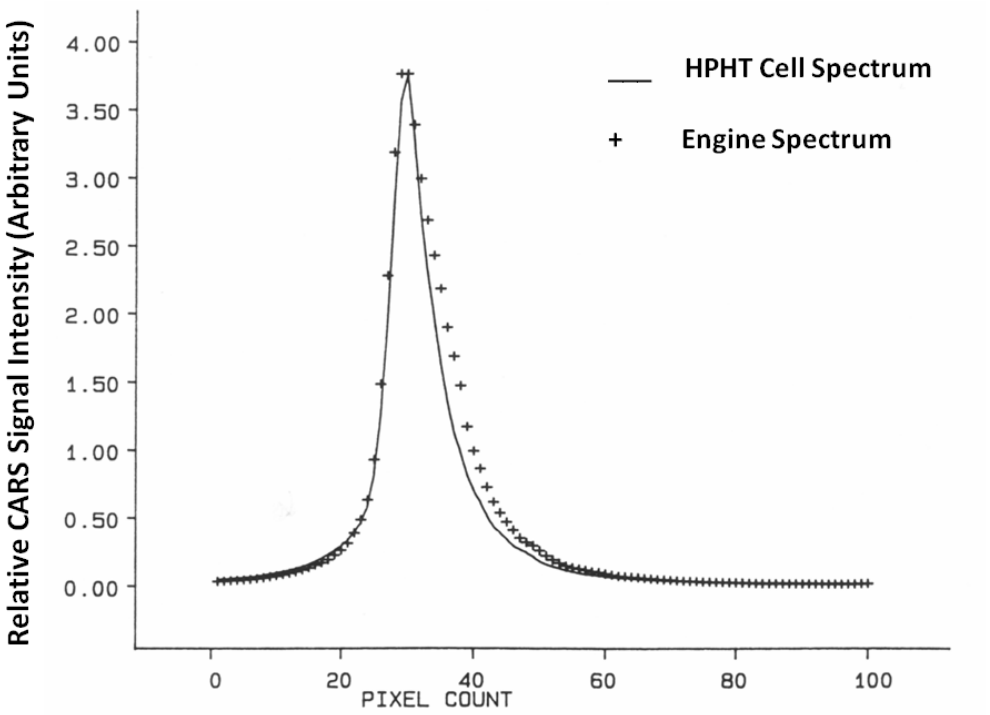

Figure 7 (a): Mean Referenced CARS Spectrum obtained in HPHT Cell (293 K, 1 atm), compared with Mean Referenced CARS Spectrum obtained in Engine (292K, 1atm).

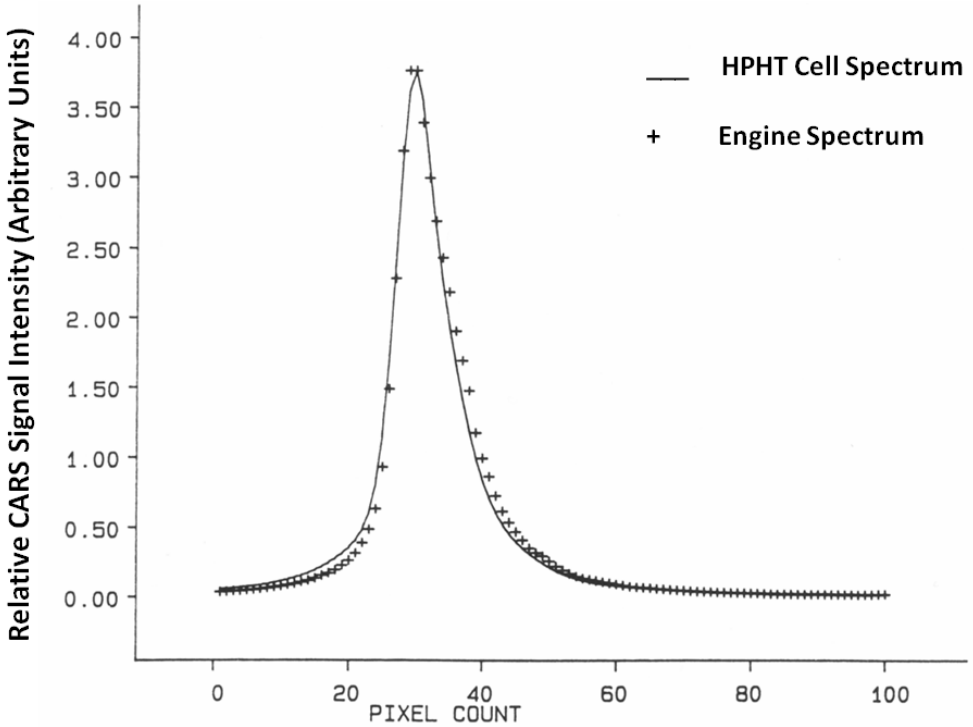

Figure 7(b): Broadened Mean Referenced CARS Spectrum obtained in HPHT Cell (293 K, 1 atm), compared with Mean Referenced CARS Spectrum obtained in Engine (292K, 1atm).

5.3 Results: Engine Temperature Measurements

5.3.1 1,000 RPM Motoring Engine Results

Figures 8, 9 and 10 show temperature histograms obtained from three complete sets of referenced single-shot CARS spectra obtained from the motored engine at 149.5^{o}, 90^{o} and 23.5^{o} before TDC respectively during the compression stroke. The histogram data shown in Figure 9 and obtained at 23.5^{o} before TDC were obtained while the engine was cold. The standard deviations imbedded in the CARS temperature distributions were approximately 39 K for all three of the datasets presented.

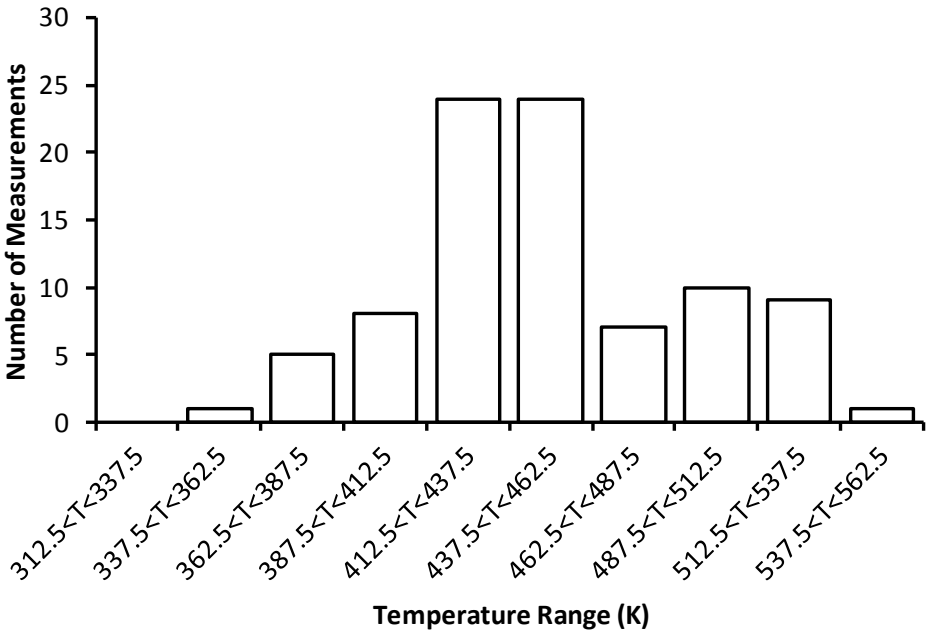

Figure 8: Distribution of 90 Single-shot CARS Temperature Measurements obtained in the Motored Ricardo E6 Engine at 150^{o} bTDC, (P = 1.25 bar ± 0.1 bar, T_{CARS} = 454 K ± 39 K).

Figure 11(a) is a graph showing the CARS air temperature measurements obtained from inside the engine as a function of crankshaft angle before and after TDC. The error bars shown for the temperature co-ordinate are one sample standard deviation obtained from the CARS spectral data, while the error bars for the crankshaft angle co-ordinate represent the uncertainty in the crankshaft angle due to fluctuations in the engine speed. Note that the temperature data at 23.5^{o} before TDC does not correspond to the histogram data presented in Figure 9. This is because the histogram

data presented in Figure 9 were obtained when the engine was cold, while the temperature data shown at the same crankshaft angle in Figure 11 (a) was obtained when the engine was warm.

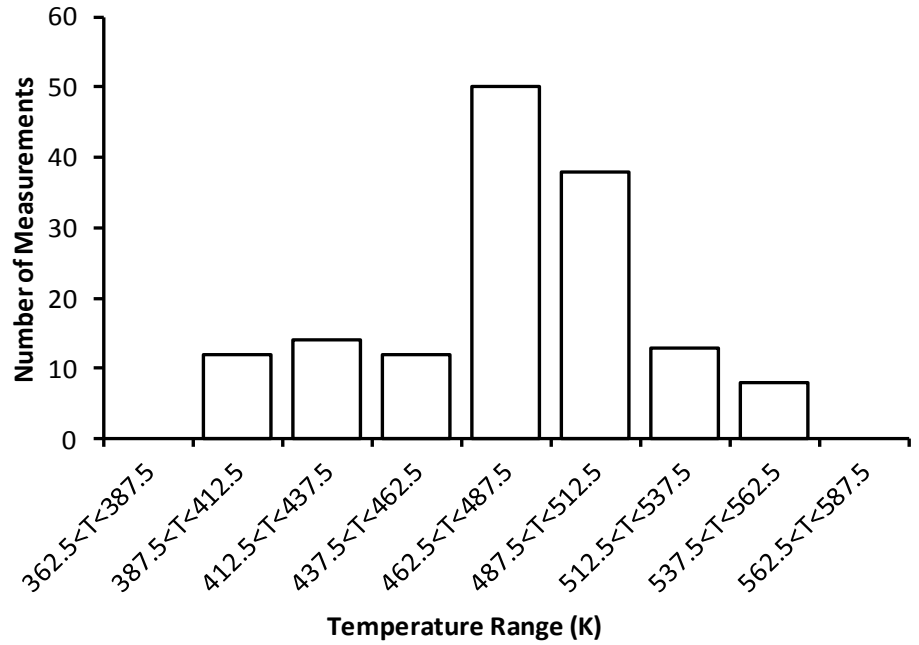

Figure 9: Distribution of 147 Single-shot CARS Temperature Measurements obtained in the Motored Ricardo E6 Engine at 90^{o} bTDC, (P = 1.7 bar ± 0.1 bar, T_{CARS} = 475 K ± 38 K).

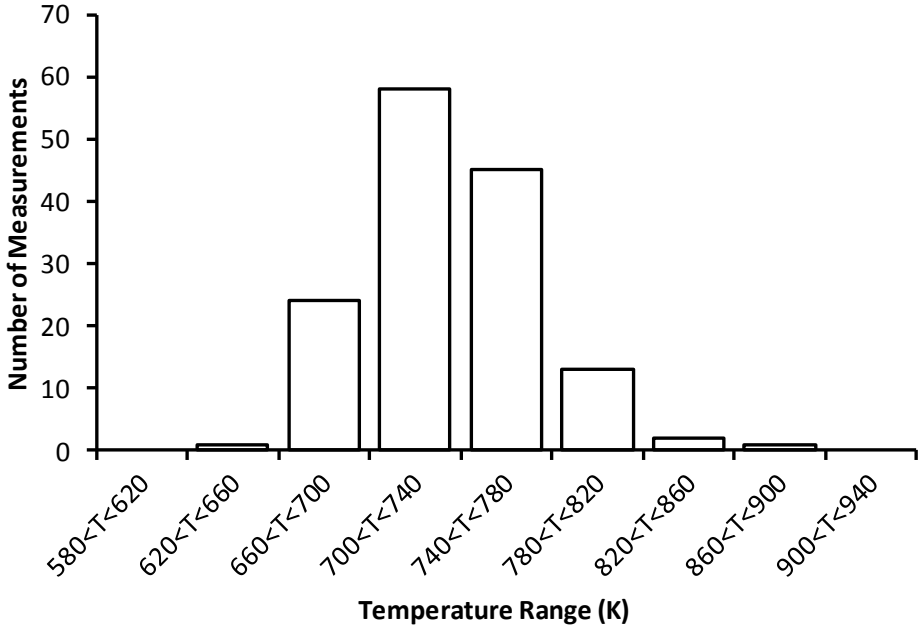

Figure 10: Distribution of 144 Single-shot CARS Temperature Measurements obtained in the Motored Ricardo E6 Engine at 23.5^{o} bTDC, (P = 11.0 bar ± 0.1 bar, T_{CARS} = 738 K ± 39 K).

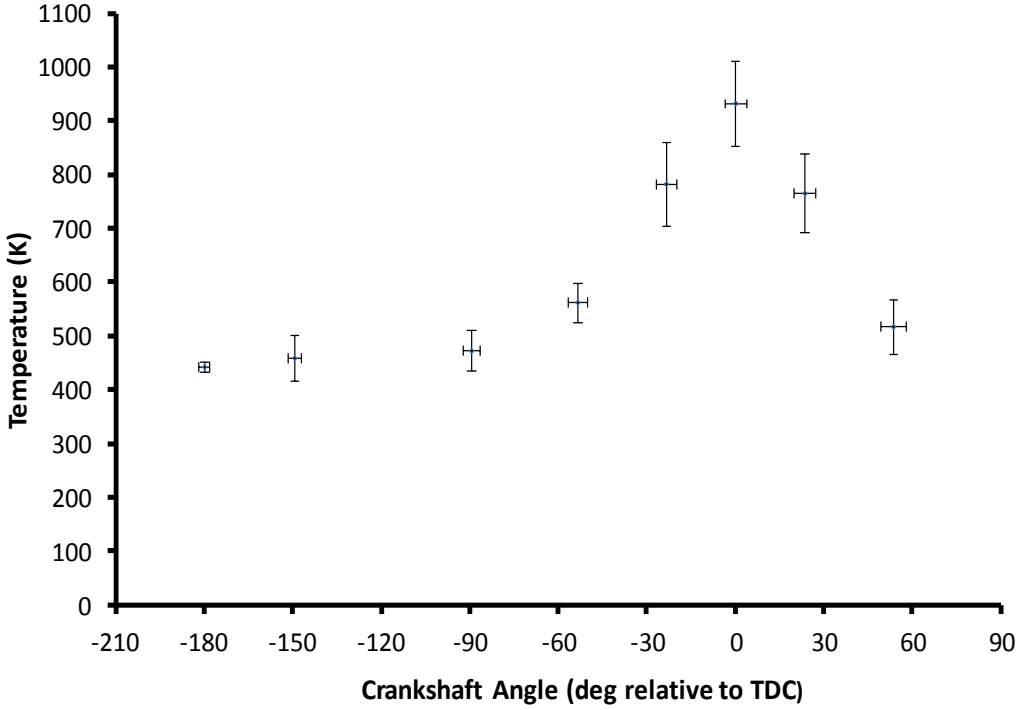

Figure 11 (a): In-Cylinder Air Temperatures as a Function of Crankshaft Angle: Engine Motored at 1,000 rpm.

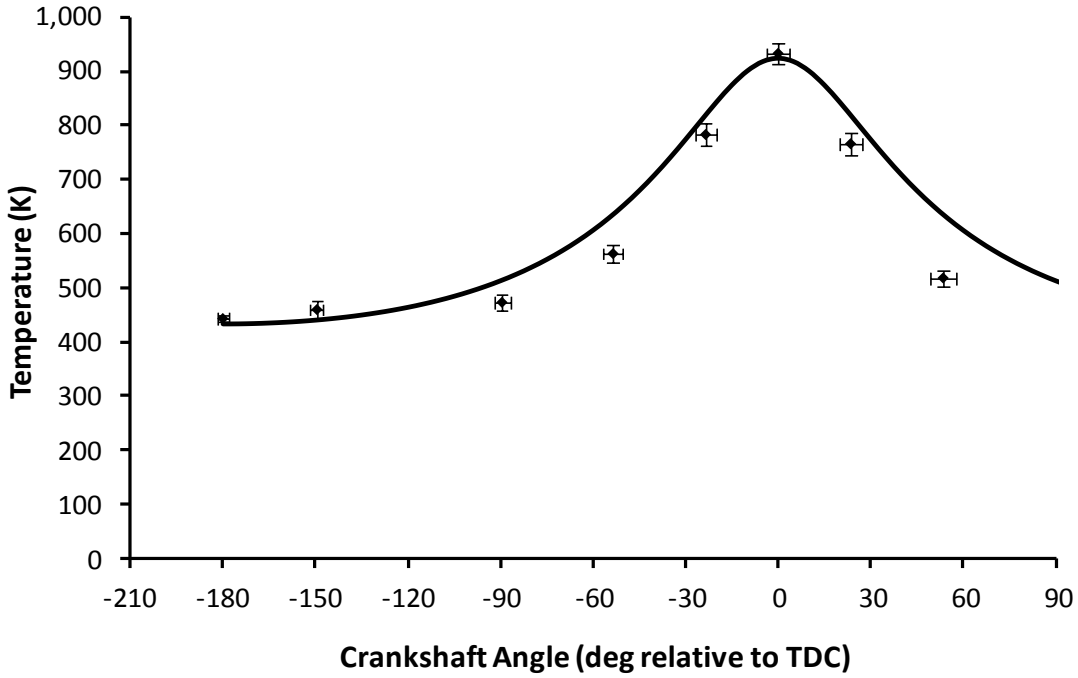

Figure 11 (b): Mean In-Cylinder Air Temperatures as a Function of Crankshaft Angle: Engine Motored at 1,000 rpm.

Figure 11 (b) presents a similar graph to that of Figure 11 (a), containing discrete temperature data and a continuous curve as a function of crankshaft angle. The discrete temperatures represent measured mean in-cylinder air temperature, and the corresponding error bars represent two standard deviations of the mean (95 % confidence interval), taken together with the absolute uncertainty in CARS temperature obtained in the HPHT cell. The error bars for the crankshaft angle represent the uncertainty in the crankshaft angle (as in Figure 11 (a) above), a result of variation in the engine speed. The continuous curve shown in Figure 11 (b) represents the best fit polytropic process relation to the experimentally obtained CARS temperatures during the compression stroke, and is discussed later in Section 6.1.

5.3.2 Methanol-Air Engine Knock Results

Following the temperature measurements of in-cylinder air during motoring at 1,000 rpm, the engine was then set to run on methanol at 1,200 rpm. The engine was run skip-fired in order to eliminate the effect of residual gas from the previous cycle on the fresh mixture. The inlet air was preheated to 443 K ± 3 K in order to facilitate engine knock every firing cycle. Once the knock signal was observed to occur during almost all the firing cycles, the inlet air temperature, ignition timing and the amount of methanol injected into the air flow was adjusted in order to control the knock intensity (indicated by the amplitude of the pressure oscillations produced in the cylinder, and measured using the pressure transducer). The inlet air temperature was reduced to 426 K ± 3 K for the 1,200 rpm measurements, and 414 K ± 3 K for the 1,400 rpm measurements, while the ignition timing was set to fire the spark plug at 34^{o} before TDC.

The carburettor was fitted with fuel nozzles suitable for methanol fuelling. The air mass flow rate and methanol mass flow rate were such as to produce a mean in-cylinder mixture equivalence ratio $\lambda = 0.91$ ($\phi = 1.09$). The methanol-air mixture formed in the inlet manifold prior to induction contained approximately 12.8 % methanol by mole. The nitrogen mole fraction in the mixture was therefore approximately 0.682. The CARS spectra obtained from the methanol-air mixture inside the engine contained a non-resonant contribution from the methanol vapour

that was absent from pure air. In addition, the molecules comprising the methanol vapour introduce new nitrogen collision partners that affect the collision line-widths in an unpredictable manner. A direct comparison of spectra obtained from nitrogen in the methanol-air mixture with nitrogen in air in the HPHT cell lead to an over-prediction of the in-cylinder mixture temperature by approximately 0 K to 50 K, dependent on the crankshaft angle and mixture pressure.

The SANDIA CARS code CARSFIT [44] was employed in order to estimate the uncertainty in the temperature measurements caused by the methanol vapour present in the fuel-air mixture, and the consequent reduction in nitrogen mole fraction obtained in the methanol-fuelled engine, relative to the air in the HPHT cell. Unfortunately, detailed collision line-width data for methanol-nitrogen molecular collisions is unavailable. In the absence of suitable line-width data, any attempt to correct for these effects will produce some error.

In order to estimate and correct for this effect, a modelled nitrogen Q-branch CARS spectral database for air was generated for the complete range of temperatures and pressures obtained in the engine, using the XMEG molecular collision line-width model [5]. Two further sets of modified CARS spectra were computed in order to account for the combined effect of the presence of methanol vapour, taken together with the reduction in nitrogen mole fraction. During the calculation of these spectra, the magnitude of the non-resonant susceptibility of the buffer gas was adjusted in order to account for the 12.8 % methanol vapour present in the methanol-air cylinder mixture. In the first set of modified spectra, the mole fraction of nitrogen and oxygen was set to 0.681 and 0.181 respectively, and the calculation was performed with N_2, O_2, CO_2 and H_2O as collision partners. The second set of modified spectra modelled the in-cylinder mixture to include nitrogen, oxygen and carbon monoxide in the same proportion as the air and methanol obtained in the engine, and the calculation was performed with N_2, O_2, and CO as collision partners. The two sets of modified CARS spectra were then compared with the database spectra calculated for nitrogen in air in order to estimate the temperature correction necessary for the actual cylinder methanol-air mixture composition. Table 4 shows the estimated temperature correction required when comparing in-cylinder spectra with HPHT cell spectra.

Table 4: Estimated Temperature Correction for Nitrogen Mole Fraction in Engine, Relative to that Obtained in the High Pressure, High Temperature Cell

Absolute Pressure (bar)	*Temperature (K)*	*CARS Temperature Correction(K) $CO/N_2/O_2$*	*CARS Temperature Correction (K) N_2/O_2*
1.0	423	- 1.0	- 1.0
4.0	550	- 6.0	- 8.5
8.0	650	- 10.0	- 18.0
12.0	750	- 18.0	- 33.0
16.0	850	- 29.0	- 42.0

Figures 12 and 13 show corrected mean methanol-air mixture temperatures obtained during the compression stroke of the knocking engine cycles, for 1,200 rpm and 1,400 rpm engine speeds respectively. Each data point represents the mean temperature obtained from approximately 150 CARS temperature measurements. The vertical error bars represent one standard deviation associated with the temperature distribution derived from the 150 single shot CARS temperatures. The vertical error bars associated with each data point shown therefore combines the variability in the CARS temperature measurements, together with the cycle-to-cycle variation in the engine. The standard deviations associated with the engine compression temperature distributions typically varied from 30 K to 60 K in magnitude.

Figure 14 shows the mean temperature measurements as a function of crankshaft angle, during the compression stroke of the knocking engine cycles, for 1,200 rpm. The temperature-crankshaft angle data points are the same as for Figure 12, but the error bars have been modified to show two standard deviations of the mean (95 % confidence interval), taken together with the absolute uncertainty in CARS temperature obtained in the HPHT cell; similar to Figure 11 (b)).

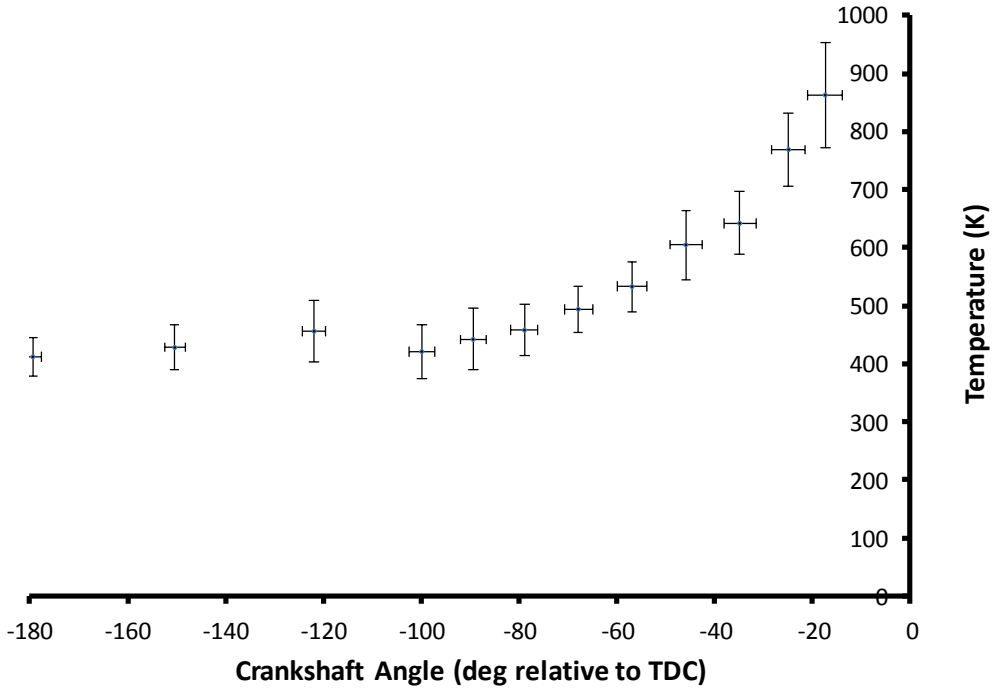

Figure 12: In-Cylinder Methanol-Air Mixture Temperature (K) as a Function of Crankshaft Angle (deg): Knocking Engine run at 1,200 rpm.

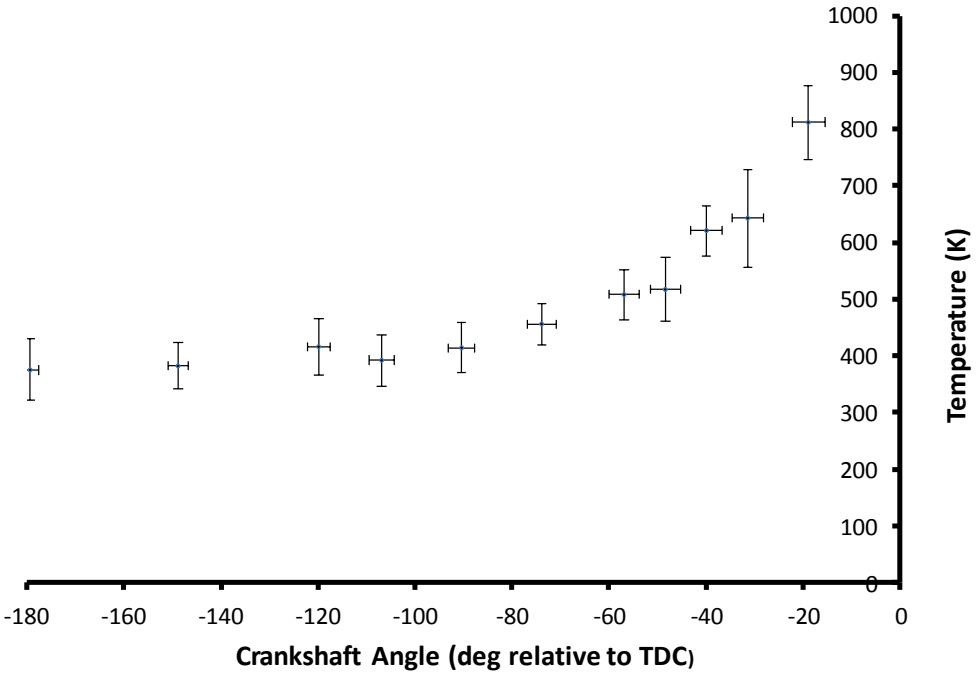

Figure 13: In-Cylinder Methanol-Air Mixture Temperature (K) as a Function of Crankshaft Angle (deg): Knocking Engine run at 1,400 rpm.

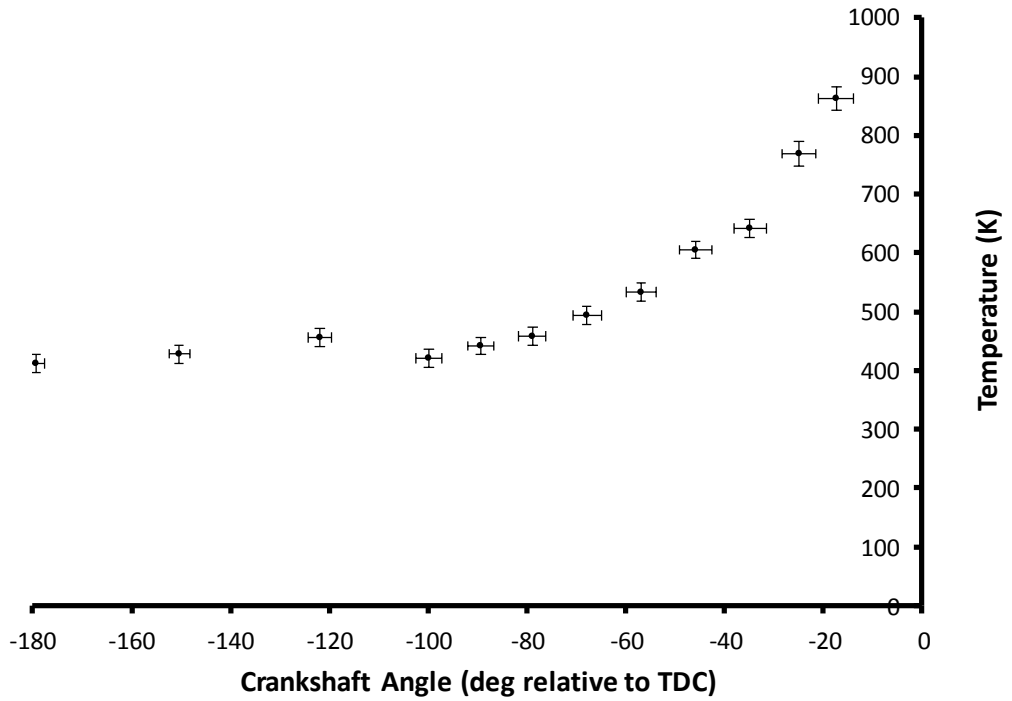

Figure 14: Mean In-Cylinder Methanol-Air Mixture Temperature (K) as a Function of Crankshaft Angle (deg): Knocking Engine run at 1,200 rpm.

5.3.3 1,000 RPM CTL Gasoline Knock Results

CTL gasoline has a lower research octane number than methanol, and hence will achieve auto-ignition conditions earlier than methanol. The inlet air temperature was reduced to approximately 80 ^{o}C, in order to reduce the intensity of the resultant engine knock. The engine was skip-fired, in order to reduce the effect of the residuals obtained from the previous firing cycles on the cycles subjected to measurement.

The SANDIA CARS code CARSFIT [43] was employed in order to compensate for the difference in nitrogen mole fraction obtained in the CTL gasoline-fuelled engine, relative to the dry air obtained in the HPHT cell. The temperature correction was discovered to be small, ranging from approximately 1 K at 1 bar to approximately 6 K at 12 bar.

Figure 15 shows the corrected, measured temperature profile of the fuel/air mixture for the engine running on CTL gasoline under knocking conditions at 1,000 rpm (the

CTL gasoline tested was comprised of approximately 75% mixed paraffin content, 15% mixed olefin content, and 10% mixed alcohol content) [42]. Each temperature data point represents the mean of approximately 150 single-shot CARS temperature measurements. The vertical error bars represent one standard deviation associated with the distribution of CARS temperatures obtained at the specified crankshaft angle. The magnitude of the error bars therefore combines the variability in the CARS temperature measurements with the cycle-to-cycle variation in the engine. The standard deviations associated with the engine compression temperature distributions typically vary from 30 K to 60 K in magnitude.

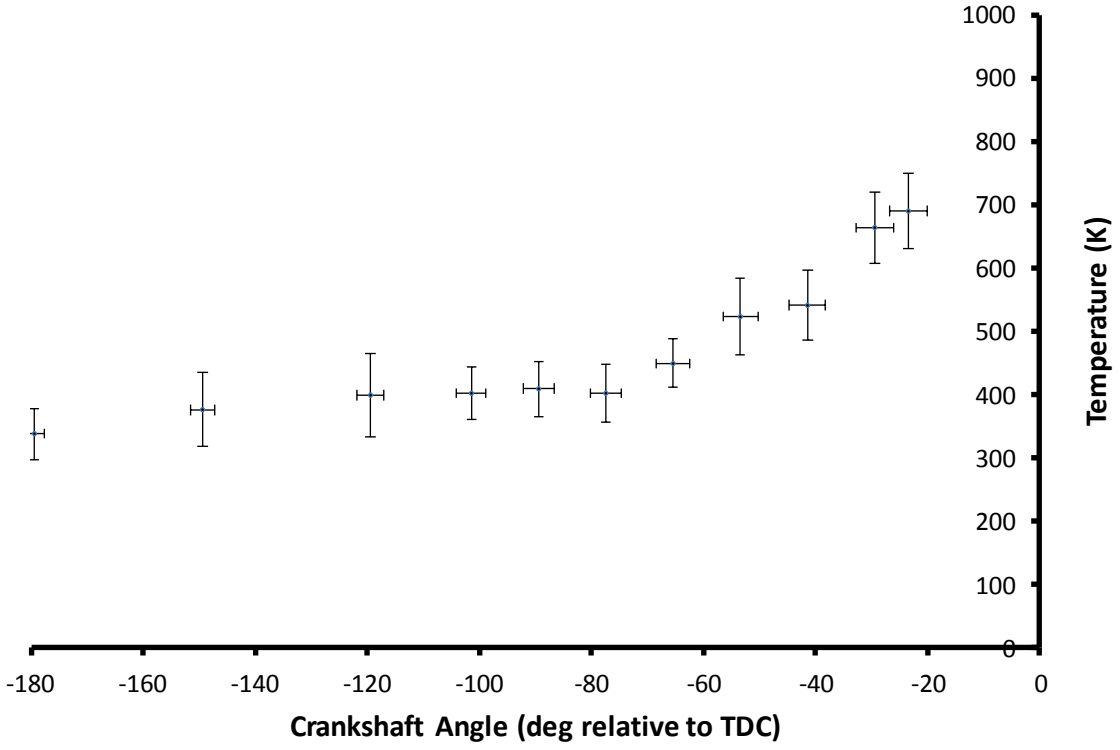

Figure 15: In-Cylinder CTL Gasoline-Air Temperature (K) as a Function of Crankshaft Angle (deg): Knocking Engine Run at 1,000 rpm.

6. Discussion: Engine Temperature Measurements

6.1 Air Temperature Profile in the Motored Engine

The compression of air in the cylinder as a function of cylinder volume is best described by a polytropic process relation. Mathematically, this is expressed by the equations

$$p(\theta) = a/V(\theta)^n; T(\theta) = b/V(\theta)^{n-1} \qquad (6.1)$$

Hence the graph of $\ln(T/T_{BDC})$ versus $\ln(V_{BDC}/V)$ is a straight line graph with a slope $m = n - 1$. A linear regression analysis performed on the compression data resulted in a best fit corresponding to $n \approx 1.336$. This value of the polytropic index n is in agreement within experimental error with the polytropic index obtained from the measured pressure-volume curve. The polytropic index n should be compared with the value that would have been obtained from a new engine using new piston rings. Perfect compression with no mass loss or heat loss would result in an adiabatic compression analysis, which results in a mean value of $k = c_p/c_v \sim 1.37$. The difference between k and n suggests that there is a small amount of blow-by in addition to the heat loss that occurs from the air to the engine block.

A comparison of the measured air temperatures during the expansion stroke with the air temperatures during the compression stroke shows the effect of heat loss from the cylinder air to the engine block. The cylinder air temperatures measured at 23.5^o after TDC and 53.5^o after TDC were significantly smaller than those measured at 23.5^o before TDC and 53.5^o before TDC respectively. This data can be used to calibrate a model of the rate of heat loss from the cylinder air to the engine block during compression and expansion.

A simple analysis of the mean temperatures at 23.5^o before TDC and 23.5^o after TDC shown in Figure 11 (b) suggests that the heat loss from the cylinder air to the engine block and the air mass loss to the sump resulted in a temperature drop of approximately 30 K, while the temperature drop occurring between 53.5^o before TDC and 53.5^o after TDC was approximately 35 K. This suggests that the net temperature

drop associated with the heat and mass loss that occurred during the compression stroke was of the order of 20 K.

6.2 Methanol-Air Temperature Profiles

A regression analysis of a polytropic compression curve fitted to the temperature-volume data presented in Figures 12 and 13 from 180^o before TDC to 34^o before TDC (corresponding to the crankshaft angle when the spark plug was fired), resulted in a polytropic index n_m ~ 1.211. This is significantly lower than the polytropic index obtained in the motored engine, and is due to the non-ideal evaporative effect of methanol on the mixture during compression.

An interesting feature of the temperature-cylinder volume profile shown in Figures 11 (a) and (b), and in Figure 14, was the effect of the hot exhaust valve and the internal fuel-air mixture flow on the measured temperature after inlet valve closure until 100^o before TDC. The fuel-air mixture in the CARS measurement volume was initially subjected to heat transfer from the hot exhaust valve, together with compression, resulting in a rise in the local temperature. Cooler fuel-air mixture transported into the measurement volume from below due to tumble, resulted in a small drop in the measured temperature between 120^o before TDC and 100^o before TDC.

The temperature profiles shown in Figures 12 and 13 show that the mean methanol-air mixture temperatures at 179.5^o before TDC were significantly larger for the 1,200 rpm case than for the 1,400 rpm case. The mean mixture temperatures at 179.5^o before TDC were measured to be 413 K ± 8 K ($2\sigma_{mean}$, 95 % confidence interval) and 376 K ± 10 K ($2\sigma_{mean}$, 95 % confidence interval) for the 1,200 rpm and 1,400 rpm cases respectively. This difference was probably due to the rate of air flow heating decreasing as the mass flow rate of air into the engine increased, and had the consequence of the 1,200 rpm temperature profile (Figure 12) following a higher temperature compression profile than the 1,400 rpm case (Figure 13).

The temperature profiles shown in Figures 11 and 12 indicated a sudden increase in the rate of change of temperature with crankshaft angle following spark ignition. This was to be expected, as the expanding flame, together with the moving piston,

compressed the unburned mixture. For the 1,200 rpm case, the mean temperature of the unburned mixture was measured to be 643 K ± 9 K ($2\sigma_{mean}$, 95 % confidence interval), at 35^o before TDC, increasing to a mean temperature of 864 K ± 15 K ($2\sigma_{mean}$, 95 % confidence interval) at 17.5^o before TDC following spark ignition.

For the 1,400 rpm case, the mean temperature of the unburned mixture was measured to be 622 K ± 8 K ($2\sigma_{mean}$, 95 % confidence interval), at 40^o before TDC, increasing to a mean temperature of 813 K ± 10 K ($2\sigma_{mean}$, 95 % confidence interval) at 19^o before TDC following spark ignition. The reason for the difference in temperatures at 17.5^o before TDC for the 1,200 rpm case and at 19^o before TDC for the 1,400 rpm case lies in the initial temperatures that these mixtures began with at Bottom Dead Centre (BDC), near inlet valve closure, and the subsequent polytropic compression.

The temperature profiles shown in Figures 12 and 13, together with the corresponding pressure profiles, may be employed as input in the chemical kinetic modelling of methanol-air auto-ignition, as part of a developing detonation model of the knock process. An extrapolation based on a modelled adiabatic compression of the unburned methanol-air mixture to the knock point as specified by the pressure curve predicts a maximum pre-auto-ignition temperature of approximately 1,040 K ± 20 K.

6.3 CTL Gasoline-Air Temperature Profile

A regression analysis of a polytropic compression curve fitted to the temperature-pressure data based on the temperatures presented in Figure 12 from 180^o before TDC to 41.5^o before TDC, resulted in a polytropic index n_{CTL} ~ 1.307. This was slightly smaller than the polytropic index obtained in the motored engine, and was due to the small thermodynamic cooling effect the CTL gasoline had on the cylinder air during compression.

Figure 15 shows the measured temperature profile as a function of crankshaft angle for the compression stroke for the knocking cycles. A comparison of Figure 15 with Figures 12 and 13 reveals that the final measured temperature for the CTL gasoline-air mixture at 23.5^o before TDC was approximately 687 K ± 10 K ($2\sigma_{mean}$, 95 % confidence interval). This is approximately 80 K lower than the corresponding

temperature shown in Figures 12 and 14, and approximately 70 K lower than the corresponding temperature shown in Figure 13. This is a consequence of the lower initial mixture temperature at Bottom Dead Centre, which was measured to be 339 K ± 7 K ($2\sigma_{mean}$, 95 % confidence interval), and the subsequent effect of polytropic compression.

An analysis of Figure 15 shows that the fuel-air mixing effect that caused a temperature drop at approximately 110^{o} before TDC (observable in Figures 10 and 11, and discussed earlier in Section 6.2) appears to be weaker in the engine running on CTL gasoline, compared with the same engine running on methanol. This was to be expected as the operating air-fuel ratio was much larger for CTL gasoline than for methanol, reducing the magnitude of the temperature difference effect. However, the effect remained, and the cold flow from below appeared to mix with the warmer mixture over the crankshaft angle range of 110^{o} to 77^{o} before TDC.

These results reveal that the CTL gasoline-air mixture in the engine has a significantly lower auto-ignition temperature than the corresponding methanol-air mixture. An extrapolation based on polytropic compression of the unburned CTL gasoline-air mixture to the knock point as specified by the pressure curve predicts a maximum pre-auto-ignition temperature of approximately 1,020 K ± 20 K. This is slightly smaller than the maximum pre-auto-ignition temperature predicted for the methanol-air mixture in Section 6.2. The difference of approximately 20 K may be explained by the extra time available to the CTL-air mixture to achieve the maximum pre-auto-ignition temperature as a result of the 1,000 rpm engine speed relative to the 1,200 rpm and 1,400 rpm engine speed for the methanol-air mixtures. The small difference in the predicted maximum pre-auto-ignition temperatures also suggests that the chemical mechanism responsible for hot auto-ignition may be the same for both fuels tested (methanol and CTL gasoline).

7. Conclusion

CARS temperature measurements in combustion environments are usually conducted using least squares fitting techniques applied to sets of many single-shot experimental spectra, which are fitted to a database of modelled spectra. This paper reports a

CARS temperature measurement methodology which involved the comparison of experimental CARS spectra obtained from a high pressure combustion environment (spark ignition Otto engine) with spectra obtained from a calibrated high pressure, high temperature (HPHT) cell. The matching of the spectra was conducted using a cross-correlation method, which was derived from the minimisation of the sum of normalised squares of residuals. The use of cross-correlation methods has several advantages over the minimisation of the sum of normalised squares of residuals.

The normalised cross-correlation function is: (1) linear in the dependence on the values comprising the two functions subject to comparison; (2) robust against random noise present in one or both functions; (3) provides an objective measure of goodness-of-fit; and (4) has useful Fourier properties, enabling the fast determination of multiple cross-correlations in the frequency domain.

Mode competition between modes in the dye laser caused typical standard deviations in the measured temperatures in the HPHT cell to range from 25 K to 45 K, depending on the local temperature and pressure obtained in the cell. These data extrapolated to an overall single-shot uncertainty in the local air temperature in the HPHT cell of approximately 4.5 %.

Co-linear CARS has been employed to determine the local gas temperature near the centre of the combustion chamber, 6 mm below the roof of a skip-fired optically accessible Ricardo E6 engine. Gas temperature profiles have been measured in the engine as a function of crankshaft angle for a number of cases: (1) compression and expansion stroke in the motored engine at 1,000 rpm, (2) compression stroke in the knocking methanol fuelled engine running at 1,200 rpm and 1,400 rpm respectively, and (3) compression stroke in the knocking CTL gasoline fuelled engine running at 1,000 rpm.

Cycle-to-cycle variation in the engine has combined with dye laser mode competition to create typical standard deviations in the measured gas temperatures in the engine to range from 35 K to 60 K. These data extrapolated to an overall single-shot uncertainty in the local fuel-air mixture temperature in the engine of approximately 7 %.

The CARS temperature data in the HPHT cell and in the engine were employed to determine the sample mean, and the standard deviation of the mean. The standard deviation of the mean facilitated the determination of the mean local temperatures achieved in the HPHT cell and in the engine to within 15 K to 20 K, depending on the temperature and pressure achieved in the engine.

The temperature measurements have been employed to identify the mixing of hot and cold gas in the measurement volume due to local exhaust valve heating and cold tumble flow mixing. This effect has been observed in all three examples of engine fuelling presented.

Finally, extrapolation of the temperature profiles has enabled the estimation of the maximum local temperatures achieved immediately prior to auto-ignition. In the methanol-fuelled engine, a modelled adiabatic extrapolation of the temperature to the knock point suggests that the local maximum pre-auto-ignition temperature was approximately 1,040 K ± 20 K, while in the CTL gasoline fuelled engine, a polytropic extrapolation of the temperature data to the knock point suggests that the local maximum pre-auto-ignition temperature was approximately 1,020 K ± 20 K.

Acknowledgements

The work reported in this paper was funded by the Foundation for Research Development, and the National Energy Council, Republic of South Africa. The authors would also like to acknowledge P. Ewart (University of Oxford), who facilitated the use of CARSFIT for the modelled background signal correction.

References

1. J. Sala, J. Bonamy, D. Robert, G. Millot, B. Lavorel and H. Berger, A rotational thermalization model for the calculation of collisionally narrowed isotropic raman scattering spectra - application to the SRS N_2 Q-branch, Chemical Physics 106 (1986) 427 - 439.

2. L. Rahn and R. Palmer, Studies of Nitrogen Self-Broadening at High Temperature with Inverse Raman Spectroscopy, Journal of the Optical Society of America B: v3, no.9 (1986) 1164 - 1169.

3. M. Alden, P.E. Bengtsson, and H. Edner, Rotational CARS: A Comparison of Different Techniques with Emphasis on Accuracy in Temperature Determination, Applied Optics 28 (1989) 3206 - 3219.

4. D.A. Greenhalgh, Quantitative CARS Spectroscopy, Advances in Non-Linear Spectroscopy, Eds R.J.H. Clark and R.E. Hester, John Wiley, London (1988) 193 - 251.

5. M. Woyde, and W. Stricker, The Application of CARS for Temperature Measurements in High Pressure Combustion Systems, Applied Physics B 50 (1990) 519 - 525.

6. L.P Goss, CARS Instrumentation for Combustion Applications, in Instrumentation for Flows with Combustion, ed A. Taylor, Academic Press Ltd, London (1993) 251 - 322.

7. R.L. Farrow, P.L. Mattern, and L.A. Rahn, Comparison Between CARS and Corrected Thermocouple Temperature Measurements in a Diffusion Flame, Applied Optics 21 (1982) 3119 - 3125.

8. L.R. Boedeker and G.M. Dobbs, CARS Temperature Measurements in Sooting, Laminar Diffusion Flames, Combustion Science and Technology 46 (1985) 301 - 323.

9. W. Kreutner, W. Stricker, and T. Just, Comparison of Spontaneous Raman and CARS Measurements in a Laminar Flame at Atmospheric Pressure, Applied Spectroscopy 41 (1987) 98 - 106.

10. P.E. Bengtsson, L. Martinsson, M.Alden, and S. Kroll, Rotational CARS Thermometry in Sooting Flames, Combustion Science and Technology 81 (1992) 129 - 140.

11. I.A. Stenhouse, D.R. Williams, J.B. Cole, and M.D. Swords, CARS Measurements in an Internal Combustion Engine, Applied Optics 18, (1979) 3819 - 3825.

12. D. Klick, K.A. Marko, and L. Rimai, Broadband Single-Pulse CARS Spectra in a Fired Internal Combustion Engine, Applied Optics 20 (1981) 1178 - 1181.

13. G. Alessandretti and P. Violino, Thermometry by CARS in an Automobile Engine, Journal of Physics D: Applied Physics 16 (1983) 1583 - 1594.

14. R.P. Lucht, R.E. Teets, R.M. Green, R.E. Palmer, and C.R. Ferguson, Unburned Gas Temperatures in an Internal Combustion Engine. I: CARS Temperature Measurements, Combustion Science and Technology 55 (1987) 41 - 61.

15. M.J. Cottereau, F. Grisch, and J.J. Marie, CARS Measurements of Temperature and Species Concentrations in an IC Engine, Applied Physics B 51 (1990) 63 - 66.

16. P.E. Bengtsson, L. Martinsson, M.Alden, B. Johansson, B. Lassesson, K. Marforio, and G. Lundholm, Dual-Broadband Rotational CARS Measurements in an IC Engine, 25th Symposium (International) on Combustion, The Combustion Institute (1994) 1735 - 1742.

17. G. Kalghatgi, P. Snowdon, and C.R. McDonald, Studies of Knock in a Spark Ignition Engine with CARS Temperature Measurements and Using Different Fuels, SAE 950690 (1995).

18. R. Bedue, P. Gastebois, R. Bailly, M. Pealat, and J.P.Taran, CARS Measurements in a Simulated Turbomachine Combustor, Combustion and Flame 57 (1984) 141 - 153.

19. A.C. Eckbreth, G.M. Dobbs, J.H. Stufflebeam, and P.A. Tellex, CARS Temperature Measurements and Species Measurements in Augmented Jet Engine Exhausts, Applied Optics 23, (1984) 1328 - 1339.

20. T.J. Anderson and A.C. Eckbreth, CARS Temperature/Multi-Species Measurement Strategies for Airbreathing and Rocket Propulsion Testing, 23rd Symposium (International) on Combustion, The Combustion Institute (1990) 1885 - 1891.

21. M.W. Smith, O. Jarrett, R.R. Antcliff, G.B. Northam, A.D. Cutler, and D.J. Taylor, Coherent Anti-Stokes Raman Spectroscopy Temperature Measurements in a Hydrogen-Fueled Supersonic Combustor, Journal of Propulsion and Power 9, (1993) 163 - 168.

22. A.M. Ferrario, and C. Malvicini, Real Time CARS Spectroscopy in a Semi-Industrial Furnace, Paper WD2, CLEO'83 Meeting, Baltimore (1983).

23. M. Alden, and S. Wallin, CARS Experiments in a Full Scale (10m x 10m) Industrial Coal Furnace, Applied Optics 24 (1985) 3434 – 3437.

24. P.M. Hughes, R.J. Lacelle, and T. Parameswaran, A Comparison of Suction Pyrometer and CARS Derived Temperatures in an Industrial Scale Furnace, Combustion Science and Technology 105 (1995) 131 – 145.

25. A.C. Eckbreth, Chapter 6, in Laser Diagnostics for Combustion Temperature and Species 2nd Edition, Publishers: Taylor and Francis, (1996) 281 – 379.

26. W.P. Stricker, Ch. Measurement of Temperature in Laboratory Flames and Practical Devices, in Applied Combustion Diagnostics, (ed. K. Kohse-Höinghaus and J. Jeffries), Taylor & Francis (2002) 155 – 193.

27. S. Roy, J.R. Gord, and A.K. Patnaik, Recent advances in coherent anti-Stokes Raman scattering spectroscopy: Fundamental developments and applications in reacting flows, Progress in Energy and Combustion Science 36 (2010) 280 - 306.

28. P. Snowdon, S. Skippon, and P. Ewart, Improved precision of single-shot temperature measurements by broadband CARS by use of a modeless laser, Applied Optics 30 (1991) 1008 - 1010.

29. J.P. Kuehner, M.A. Woodmansee, R.P. Lucht, J.C. Dutton, High-resolution broadband N_2 coherent anti-Stokes Raman spectroscopy: comparison of measurements for conventional and modeless broadband dye lasers, Applied Optics 42 (2003) 6757 – 6767.

30. J. Bood, P-E. Bengtsson, T. Dreier, Rotational coherent anti-Stokes Raman spectroscopy (CARS) in nitrogen at high pressures (0.1–44 MPa): experimental and modelling results, Journal of Raman Spectroscopy 31 (2000) 703 – 710.

31. M. Afzelius, P.-E. Bengtsson, J. Bood, J. Bonamy, F. Chaussard, H. Berger, T. Dreier, Dual-broadband rotational CARS modelling of nitrogen at pressures up to 9 MPa. II. Rotational Raman line widths, Applied Physics B 75 (2002) 771 - 778.

32. C.J. Kliewer, A. Bohlin, E. Nordström, B.D. Patterson, P-E. Bengtsson, T.B. Settersten, Time-domain measurements of S-branch N_2–N_2 Raman line-widths using

picosecond pure rotational coherent anti-Stokes Raman spectroscopy, Applied Physics B 108 (2012) 419 - 426.

33. B. Grandin, I. Denbratt, J. Bood, C. Brackmann, P-E. Bengtsson, The Effect of Knock on the Heat Transfer in an SI Engine: Thermal Boundary Layer Investigation using CARS Temperature Measurements and Heat Flux Measurements, SAE Technical Paper 2000-01-2831, 2000.

34. M. Weikl, F. Beyrau, A. Leipertz, Simultaneous temperature and exhaust-gas recirculation-measurements in a homogeneous charge-compression ignition engine by use of pure rotational coherent anti-Stokes Raman spectroscopy, Applied Optics 45 (2006) 3646 - 3651.

35. F. Beyrau, M. Weikl, T. Seeger, A. Leipertz, Application of an optical pulse stretcher to coherent anti-Stokes Raman spectroscopy, Optics Letters 29:20 (2004) 2381 - 2383.

36. A. Birkigt, K. Michels, J. Theobald1, T. Seeger, Y. Gao, M. Weikl, M. Wensing, A Leipertz, Investigation of compression temperature in highly charged spark-ignition engines, International Journal of Engine Research 12 (2011) 282 - 292.

37. R.D. Lockett, CARS temperature measurements and chemical kinetic modelling of auto-ignition in a methanol fuelled internal combustion engine, PhD Thesis, University of Cape Town, Rondebosch, Republic of South Africa (1993).

38. G. N. Robertson and A. Roblin, Analysis of CARS spectra using Fourier transform techniques, in Coherent Raman Spectroscopy: Applications and New Developments, E. Castellucci, R. Righini, and P. Foggi, eds. World Scientific, Singapore (1993) 39 – 42.

39. M. Schenk, A. Thumann, T. Seeger, and A. Leipertz, Pure rotational coherent anti-Stokes Raman scattering: comparison of evaluation techniques for determining single-shot simultaneous temperature and relative N2-O2 concentration, Applied Optics 37:24 (1998) 5659 - 5671.

40. S. Green, P. Rubas, M. Paul, J. Peters, R. Lucht, Annular phase matched dual-pump coherent anti-Stokes spectroscopy system for the simultaneous detection of nitrogen and methane, Applied Optics 37:9 (1998) 1690 - 1701.

41. F. Beyrau, T. Seeger, A. Malarski, A. Leipertz, Determination of temperaturees and fuel/air ratios in an ethene-air flame by dual-pump CARS, Journal of Raman Spectroscopy 34:12 (2003) 946 - 951.

42. D. Ball, H.S.T Driver, R.J. Hutcheon, R.D. Lockett, G.N. Robertson, CARS Temperature Measurements in an Internal Combustion Engine, Optical Engineering 33 (1994) 2870 – 2874.

43. S. Kroll, M. Alden, T. Berglind, R.J. Hall, Noise characteristics of single shot broadband Raman-resonant CARS with single- and multimode lasers, Applied Optics 26 (1987) 1068 – 1073.

44. Palmer, R. E., The CARSFT Computer Code for Calculating Coherent Anti-Stokes Raman Spectra: User and Programmer Information, Sandia National Laboratories Report SAND89-8206, Livermore, California, 1989.